AFCRC-TR-58-228(I)
ASTIA Document No. AD 152509

GEOPHYSICAL RESEARCH PAPERS
No. 58

THEORY OF LARGE-SCALE ATMOSPHERIC DIFFUSION AND ITS APPLICATION TO AIR TRAJECTORIES

VOLUME I

SAMUEL B. SOLOT
and
EUGENE M. DARLING, JR.

June 1958

PROJECT 7616

Atmospheric Analysis Laboratory
GEOPHYSICS RESEARCH DIRECTORATE
AIR FORCE CAMBRIDGE RESEARCH CENTER
AIR RESEARCH AND DEVELOPMENT COMMAND
UNITED STATES AIR FORCE
BEDFORD, MASS.

FOREWORD

This Geophysics Research Paper is published in three separate volumes.

In Volume I, the theory of large-scale atmospheric diffusion is developed. The application of this theory to air trajectories is presented in Volumes II and III.

Volume II contains probability tables for various constant values of mean zonal wind.

Volume III consists of probability tables for North America and Eurasia.

ACKNOWLEDGEMENT

The authors wish to express their sincere appreciation to Messrs. Robert E. Chabot and Joseph Hess who performed the laborious hand calculations required to prepare the basic data for machine computation.

ABSTRACT

G. I. Taylor's theory of diffusion by continuous movement is adapted to motions on the scale of the general circulation. The resultant theory pertains to diffusion, by large-scale eddies, of air particles constrained to move on a constant-level surface. This theory provides a means for determining the probability field as a function of time for a particle originating from a given point on the surface of a sphere.

The bivariate normal density function describes the probability of a displacement with components x (West - East) and y (North - South). This function reduces to the circular normal form when suitable empirical and theoretical simplifications are introduced, concerning the mean zonal wind, the standard deviation of displacement components, and the correlation between displacement component deviations.

This density function is integrated in polar form and mapped on a projection of the earth's surface by means of a suitable spherical transformation. The resulting form of the distribution function is applicable to problems of atomic fallout.

In applying diffusion theory to balloon operations, the concept of downstream probability density function is introduced. This function defines the probability density with respect to latitude of an East-West displacement at least as large as a specified value, occurring within T days. Tables of the downstream probability function are presented in Volumes II and III for (a) various constant values of mean wind and (b) North America and Eurasia for January, April, July, and October at 40,000 to 80,000 feet.

CONTENTS

ILLUSTRATIONS

ILLUSTRATIONS (CONT.)

TABLES

SYMBOLS

x, y	- displacement components in the West - East and North - South directions, respectively (Note: eastward and northward displacements are taken as positive)
X, Y	- climatological mean displacements in the x and y directions, respectively
$x' = x-X$	- displacement component deviation in the West - East direction
$y' = y-Y$	- displacement component deviation in the North - South direction
σ_x, σ_y	- standard deviation of x and y, respectively
σ	- standard deviation of displacements
u, v	- wind components in the x and y directions, respectively
U, V	- climatological mean winds in the u and v directions, respectively
$u' = u-U$	- wind component deviation in the West - East direction
$v' = v-V$	- wind component deviation in the North - South direction
$p(m, n)$	- bivariate normal probability density function for variables m, n
$\rho(m, n)$	- linear correlation coefficient between the variables m and n
σ_u, σ_v	- standard deviation of u and v, respectively
σ_i	- standard deviation of the wind
$G_x(T)$, $G_y(T)$	- functions which determine the time dependence of σ_x and σ_y, respectively

$$G_x(T) = \frac{\sigma_x}{\sigma_u} \qquad G_y(T) = \frac{\sigma_y}{\sigma_v}$$

$s = \sqrt{(x')^2 + (y')^2}$	- magnitude of the deviation displacement, also co-latitude in a rotated system of spherical coordinates
$v = \sqrt{(u')^2 + (v')^2}$	- magnitude of the deviation wind vector
v_0, s_0	- particular values of v and s, respectively
$\eta = \sigma_v / \sigma_u$	

SYMBOLS (CONT.)

$P(m, n)$	- bivariate normal distribution function for the variables m, n
$\bar{\lambda}$	- mean longitude displacement
λ	- longitude, measured eastward from a given initial longitude
$\lambda' = \lambda - \bar{\lambda}$	- deviation longitude
ϕ	- latitude
α	- longitude in a rotated system of spherical coordinates
$\hat{U} = \frac{\int_{\phi_o}^{\phi} U \, d\phi}{\phi - \phi_o}$	- a value of U averaged over latitude between ϕ_o, the initial latitude, and ϕ, an arbitrary latitude
$\hat{\sigma}_i = \frac{\int_{0}^{S} \sigma_i \, ds}{S}$	- a value of σ_i appropriate for the population of deviation displacements from 0 to S
DPDF	- downstream probability density function
R_ξ	- auto-correlation function
ξ	- a small time increment
t	- time
T	- time in days
a	- a constant, depending on the size of an eddy

THEORY OF LARGE-SCALE ATMOSPHERIC DIFFUSION AND ITS APPLICATION TO AIR TRAJECTORIES

1. INTRODUCTION

In recent years the constant-level balloon has developed into a vehicle of major scientific importance. Its payload may consist of a variety of measuring devices which utilize appropriate communications systems to telemeter information back to earth. In many cases this kind of data can be obtained in no other way. Indeed, even the paths of these balloons are of great scientific interest, since they represent solutions to the equations of large-scale atmospheric motions in a Lagrangean system of coordinates.

One of the most attractive features of the constant-level balloon is a direct consequence of its size. It is large enough to be insensitive to small-scale eddies, while responding freely to the large-scale motions of the atmosphere. Paradoxically, it is this very freedom of movement which imposes the most severe operational limitation on the balloon system, namely uncontrollability. The horizontal path can be controlled to a small extent in two ways: (a) by varying the time of launching, and thus predetermining the initial horizontal velocity at altitude, and (b) by varying the altitude during flight. Except for these measures, knowledge of the future positions of balloons must largely depend upon meteorological prediction.

Experience has shown that for time periods greater than a few days conventional prediction methods are unreliable. For these longer time intervals, statistical methods must be used. To be valid, such methods must be based on a set of fundamental statistics of large-scale atmospheric motions. This is but one example of the need for such statistics.

NOTE: Author's manuscript approved 19 March 1958.

Many schemes have been proposed for combined networks of balloons, launched from several sites at predetermined time intervals. Such experiments are necessarily costly and must be thoroughly evaluated. To perform an intelligent job of evaluation, one must again have access to a reliable set of statistics on atmospheric motions. In fact, the lack of such information has seriously deterred realization of the full potential value of balloon systems.

This paper presents a set of statistics on atmospheric trajectories in a form which has been found most useful for solving the problems discussed above and other related problems.

The most straightforward approach to the problem of distribution of trajectory end-points is to compute a large number of trajectories, having a common origin, from a series of upper-level charts. Here, either the observed winds or the computed geostrophic winds, or both, are used as basic data. The accuracy of such computations will depend to some extent on the time interval between successive maps. A number of such studies have been made, and these are useful in giving at least a gross estimate of the distribution functions. However, in addition to the magnitude of this task, there are three serious limitations to this approach:

a. It is extremely difficult to compute accurate trajectories.

b. With the type of data at our disposal, it is almost impossible to achieve a sample sufficiently large to be considered representative.

c. Even in those few cases where the first two limitations can be overcome, the applicability of the results is restricted to a particular region in space, a particular height, and a particular season.

With regard to the first limitation, it is only fair to state that a sufficiently large sample would overcome this restriction if there were no systematic computational errors.

The Moby Dick flights are an important source of data. Although many hundreds of balloons have been flown, only a small percentage of these flights are of sufficiently long duration to be useful. Thus the last two limitations still remain in force. Furthermore, there is a definite bias in these data because the launchings were mainly confined to selected situations when the westerlies were strongest.

From the foregoing discussion it is evident that an adequate theory of diffusion on the scale of the general circulation is needed. This paper attempts to derive such a theory. This is by no means a complete theory, since certain simplifying assumptions and approximations have been introduced. The criterion adopted in introducing these approximations was to maintain compatibility between the degree of refinement of the theory and the quality of the input data.

Any theory of diffusion of air particles by the general circulation eddies must provide a means for determining the probability field as a function of time for a particle released from a given point on a sphere's surface. Initially, the probability of the particle's location is 100 percent at the origin and 0 elsewhere. As time passes, the particle's location is specified by a probability field. After a very long period of time, the probability field tends toward uniformity over the sphere's entire surface and the particle's origin ceases to be important.

G. I. Taylor's theory of diffusion by continuous movement[1] is a solution of this problem for small-scale eddies. The theory presented here is an adaptation of Taylor's theory for motions on the scale of the general circulation. In developing our theory, we incorporated results obtained from empirical studies of the trajectory distribution function.

The probability density function can, of course, be integrated with respect to space and time in a number of ways to obtain the desired distribution function. In planning the presentation of theoretical calculations, we found that each specific class of application required a particular method of integration to obtain the most useful form of the distribution function. One presentation is included which, while not very useful for constant-level balloon operations, may have important applications to the problem of diffusion of particulate matter, such as fallout from atomic weapons.

2. PROBABILITY THEORY OF DISPLACEMENTS

Consider an air particle constrained to move on a constant-level surface.

This particle is located at 0 at time t = 0 (Figure 1). What is the probability of the particle being located at point P, at t = T? (Note that in this statement of the problem we prescribe only the end-point of a displacement, not the path.) Making the usual assumption that the two displacement components, x and y, are normally distributed about their respective means, X and Y, the probability of displacement, OP, may be expressed by the equation for the bivariate normal density function:

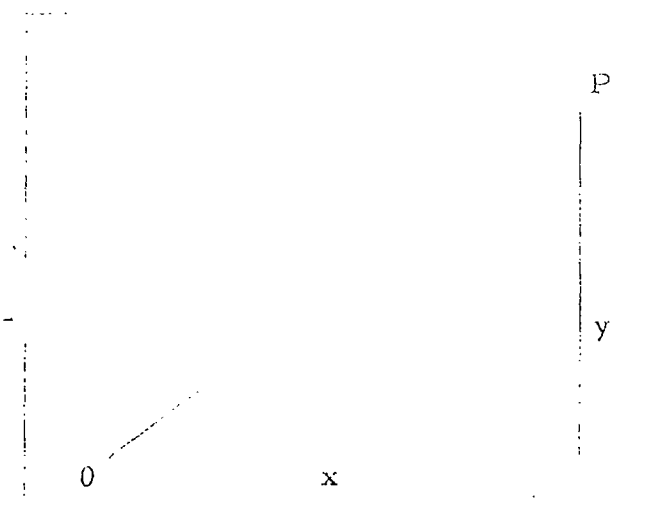

Figure 1. Displacement of an air particle

$$p(x, y) = \frac{1}{2\pi \sigma_x \sigma_y \sqrt{1-\rho^2}} \exp\left\{\frac{-1}{2(1-\rho^2)}\left[\left(\frac{x-X}{\sigma_x}\right)^2 - 2\rho\frac{(x-X)(y-Y)}{\sigma_x \sigma_y} + \left(\frac{y-Y}{\sigma_y}\right)^2\right]\right\} \quad (1)$$

where σ_x and σ_y are the standard deviation of x and y, respectively, and ρ is the coefficient of correlation between the quantities $x' = (x-X)$ and $y' = (y-Y)$. By definition

$$X = \int_0^T U\, dt \quad (2) \qquad \text{and} \qquad Y = \int_0^T V\, dt \quad (3)$$

where U and V are components of the climatological mean wind encountered by the particle in its path.

In the stratosphere and upper troposphere, V is small and difficult to determine. This is especially true in middle latitudes. In fact it may be assumed, with little loss of generality, that the mean wind in these regions is zonal. Let us now more closely examine the mean wind variation.

Table 1 is a typical sample of mean upper-level winds, taken from the Handbook of Geophysics.[2] Note that the variation is considerably greater with respect to latitude than with respect to longitude.

Table 1: Mean wind speed (knots), 50,000 ft., January

LATITUDE	WEST LONGITUDE				LONGITUDE RANGE
	120	100	80	60	
70	34	33	33	34	1
60	36	29	26	29	10
50	38	41	44	43	6
40	71	84	83	67	17
30	61	58	48	37	24
LAT RANGE	37	55	57	38	

It is evident that if we confine our discussion to specific geographical regions, to a reasonable approximation, we need only consider the latitudinal variation of the mean wind. Therefore, we introduce the following modeling approximations:

$$Y = V = 0 \qquad (4) \quad \text{and} \quad U = U_{i,\,j,\,k}(\phi) \qquad (5)$$

where i, j, and k are height, season, and geographical region (such as North America, Eurasia, etc.), respectively, and ϕ is latitude.

It can be shown theoretically that $\rho(x', y')$, the coefficient of correlation between the displacement components, is proportional to $\rho(u', v')$, the correlation coefficient between the wind components, where $u' = (u-U)$, and $v' = v$. Brooks, et al,[3,4] Buch,[5] and Court[6] conducted independent studies of statistical properties of the winds in the free atmosphere over broad regions. All three authorities agree that $\rho(u', v')$ is small. Table 2 is a typical example extracted from Court's paper.

Table 2: Coefficient of correlation between u and v

HT. (km)	PANAMA CANAL ZONE		MT. CLEMENS, MICH.		GOOSE BAY, LAB.	
	Winter	Summer	Winter	Summer	Winter	Summer
0	.000	.124	.054	.051	-.119	.022
10	.075	.041	.091	.050	-.087	.027
20	.059	-.174	.129	-.154	.112	-.063

In Eq. (1), ρ^2, which appears in both denominator and exponent, must be compared to unity. Since the first and last terms in the exponent within the brackets are of the same order, the value of ρ within the bracket must be compared to unity. From a complete study of the evidence it becomes apparent that, compared to 1, ρ is small and ρ^2 is very small. Thus we introduce the assumption that

$$\rho = 0 \tag{6}$$

The time dependence of σ_x and σ_y is fully discussed in Appendix III where the equations $\sigma_x = G_x(t)\sigma_u$ and $\sigma_y = G_y(t)\sigma_v$ are developed. It is also shown in Appendix III that empirical evidence warrants the assumption that $G_x(t) = G_y(t)$. Therefore, it is evident that $\sigma_y = q\sigma_x$ where q is the ratio $\frac{\sigma_v}{\sigma_u}$.

Consider now the quantities σ_u and σ_v. With the sample sizes generally available, σ_u can be determined with much greater precision than σ_v. Therefore, it is reasonable to assume that any error in the estimated value of q will be reflected in σ_y rather than in σ_x. Let us then investigate the consequences of assuming that $q = 1$. If q is actually greater than 1, then the dispersion in the y-direction is greater than we have assumed. On the other hand, if q is actually smaller than 1, then we have overestimated the dispersion in the y-direction.

In applying the theory to balloon systems, we are usually interested in obtaining the greatest possible concentration (that is, least dispersion) of displacements. As will be shown later, the results of several studies indicate that, in general, $q > 1$. Thus it may be seen that any errors resulting from the $q = 1$ assumption will be in the conservative direction when the theory is applied to balloon systems. We will now discuss the magnitude of these errors.

Brooks, et al.[3,4] extensively investigated σ_u and σ_v and concluded that there was no significant difference between these quantities in the free atmosphere. Buch[5] conducted a detailed investigation, on a hemispheric basis, of the wind statistics for a single year. His findings agree with those

of Brooks' in middle and high latitudes. However, he found that in low latitudes q is significantly less than 1. Court's[6] more recent studies show that there is a consistent variation of q with elevation at widely separated stations. The ratio, q , is 1 at the Jet Stream level (about 40,000 ft) and decreases gradually with increasing elevation. Court also found that this effect is very pronounced at low latitudes, but it is much smaller at middle and high latitudes. Let us confine our attention to middle and high latitudes and to elevations between 40,000 and 80,000 feet. All authorities mentioned above agreed that the error in assuming $\sigma_v = \sigma_u$ is negligible at 40,000 feet. Our own studies show no significant difference between σ_v and σ_u, even at 80,000 feet. These results are not necessarily in conflict with Court's data. He used data from single stations, whereas our estimates were based on populations of winds taken along single latitudes but from a number of adjacent longitudes. By definition, $\sigma_v^2 = \overline{v^2} - (\bar{v})^2$. It has already been shown that the regional value of $(\bar{v})^2$ is 0 (Eq. 4). For a single point, however, $(\bar{v})^2$ is not negligible. Therefore, other things being equal, the value of σ_v will always be larger for a region than for a single point within the region.

The foregoing discussion leads to the assumption that

$$\sigma_y = \sigma_x = \sigma \quad . \tag{7}$$

We may now rewrite Eq. (1) in various alternate forms:

$$p(x, y, t) = p(x, t)\, p(y, t) = \frac{1}{2\pi\sigma^2} \exp\left\{-\left[\frac{(x')^2 + y^2}{2\sigma^2}\right]\right\}, \tag{8}$$

$$p(x, t) = \frac{1}{\sqrt{2\pi}\,\sigma} \exp\left[-\frac{(x')^2}{2\sigma^2}\right] \quad , \tag{9}$$

$$p(y, t) = \frac{1}{\sqrt{2\pi}\,\sigma} \exp\left[-\frac{y^2}{2\sigma^2}\right] \quad . \tag{10}$$

We may write Eq. (8) in polar form by introducing $s^2 = (x')^2 + y^2$ and integrating from 0 to 2π :

$$p(s, t) = \frac{s}{\sigma^2} \exp\left[-\frac{s^2}{2\sigma^2}\right] \quad . \tag{11}$$

The preceding equations are familiar forms of the circular normal density function. Brooks, et al,[3,4] used these equations to compute the probability of winds.

3. ANALOGY BETWEEN THE WIND PROBLEM AND THE DISPLACEMENT PROBLEM

The displacement problem can be viewed as a logical extension of the wind problem. We will compare the solutions to these two problems at every step to illustrate their relationship. In this analogy we will retain the simplifying assumptions and approximations which have already been established.

The appropriate wind equations which correspond to Eqs. (8), (9), (10), and (11) are:

$$p(u,v) = p(u)\,p(v) = \frac{1}{2\pi\sigma_i^2}\exp\left\{-\left[\frac{(u')^2+v^2}{2\sigma_i^2}\right]\right\}, \qquad (8a)$$

$$p(u) = \frac{1}{\sqrt{2\pi}\,\sigma_i}\exp\left[-\frac{(u')^2}{2\sigma_i^2}\right], \qquad (9a)$$

$$p(v) = \frac{1}{\sqrt{2\pi}\,\sigma_i}\exp\left[-\frac{v^2}{2\sigma_i^2}\right], \qquad (10a)$$

and

$$p(c) = \frac{c}{\sigma_i^2}\exp\left[-\frac{c^2}{2\sigma_i^2}\right] \qquad (11a)$$

where σ_i is the standard wind deviation and $c^2 = (u')^2 + v^2$.

We note that the independent variables for the wind equations are u and v; but for the displacement equations, in addition to x and y, the variable, t, also appears. In general both the wind and displacement probability density functions are completely specified when two primary parameters, U and σ_i, are given. However, the empirically determined relationship between U and σ_i, developed in Appendix II, reduces the required number of primary parameters to a single one, namely, U. We define secondary parameters as those

variables which represent the time and space dependence of the mean wind itself. In this paper the secondary parameters are height, season, region (in the sense defined previously), and latitude for the wind statistic and similarly, height, season, region, and initial latitude for the displacement statistic.

In the wind problem the specified wind (u, v) can be represented as a two-dimensional vector in plane surface. However, the vector x, y must be mapped on the earth's surface which is spherical. Therefore, at some point in the solution of the displacement problem we must introduce a transformation to spherical coordinates. One additional complication arises which is confined exclusively to the displacement problem. Since the component y represents a change in latitude, and since both U and σ_i are functions of latitude, we must somehow incorporate in the probability function a continuously varying population of winds. Just how we overcome these difficulties will be discussed in the next section.

4. POLAR INTEGRATION OF THE PROBABILITY DENSITY FUNCTION

Any desired form of the distribution function may be obtained by an appropriate integration of Eqs. (8) to (11) and (8a) to (11a). A useful form of the wind distribution function is derived from integration of Eq. (11a). A rather complete discussion of this function will be found in Brooks, et al.[3,4]

Integrating Eq. (11a) with respect to c:

$$P(C) = \frac{1}{\sigma_i^2} \int_0^C \exp\left[-\frac{c^2}{2\sigma_i^2}\right] c\, d\, c = 1 - \exp\left[-\frac{C^2}{2\sigma_i^2}\right] . \qquad (12a)$$

This function may be interpreted as follows: Any wind with probability, P, is the vector sum of U, the vector mean wind, and a deviation vector of magnitude, C, where

$$C = \sigma_i \left[\ln \frac{1}{1 - P(C)^2}\right]^{1/2} \qquad (13a)$$

An analogous polar integration of the displacement density function(Eq. 11) is useful in certain types of problems. To demonstrate the method of computing this form of distribution function, we will apply the theory to a specific example.

The problem we have selected is the mapping of the 0.50 probability curve for the following specifications:

Region:	North America
Height:	50,000 Feet
Season:	January
Initial Latitude:	40°N
Time:	1 Day

The profiles of U and σ_i are shown in Figure 2. As a preliminary to the discussion of the displacement function, we solve the 0.50 probability problem for the wind occurring at 40°N. We note that the mean wind at 40°N is 75 knots and the standard deviation is 35.8 knots (Figure 2). From Eq. (13a):

$$C = 35.8 \left[\ln 4 \right]^{1/2} = 35.8 \times 1.176 = 42 \text{ kts.} \qquad (14a)$$

The solution is illustrated in Figure 3. The probability of occurrence is at least 0.50 for all winds which can be represented by vectors with a common origin at 0, 0 and whose end-points lie within the designated circle. Thus the circle of radius, 42 knots, and origin at the end-point of the vector, U=75 knots, is the locus of the limiting vector end-points for a probability of 0.50. The solution consists of two independent parts: (a) a mean wind vector, U, and (b) a deviation wind vector, u', of magnitude, C. Figure 3 also clearly shows that the component $u = (U + u')$.

For the displacement distribution function we seek a similar solution, but we further require that the 0.50 probability curve be mapped on a spherical earth. For this purpose it is convenient to use one degree of latitude on the earth's surface as a unit of length, and one day as a time unit. It is also convenient to adopt a coordinate system in which λ is the longitude coordinate measured eastward from the initial longitude, and ϕ is the true latitude. Here, as in the wind problem, the solution is resolved into two independent parts: the computation of (a) a mean displacement, Λ, and (b) a deviation displacement with components λ', $(\phi - 40)$. Also, $\lambda = \Lambda + \lambda'$. As was previously stated, any displacement in latitude involves a change in both U and σ_i. Thus, unlike the wind problem where U is independent of v, in this case, Λ is a function of ϕ.

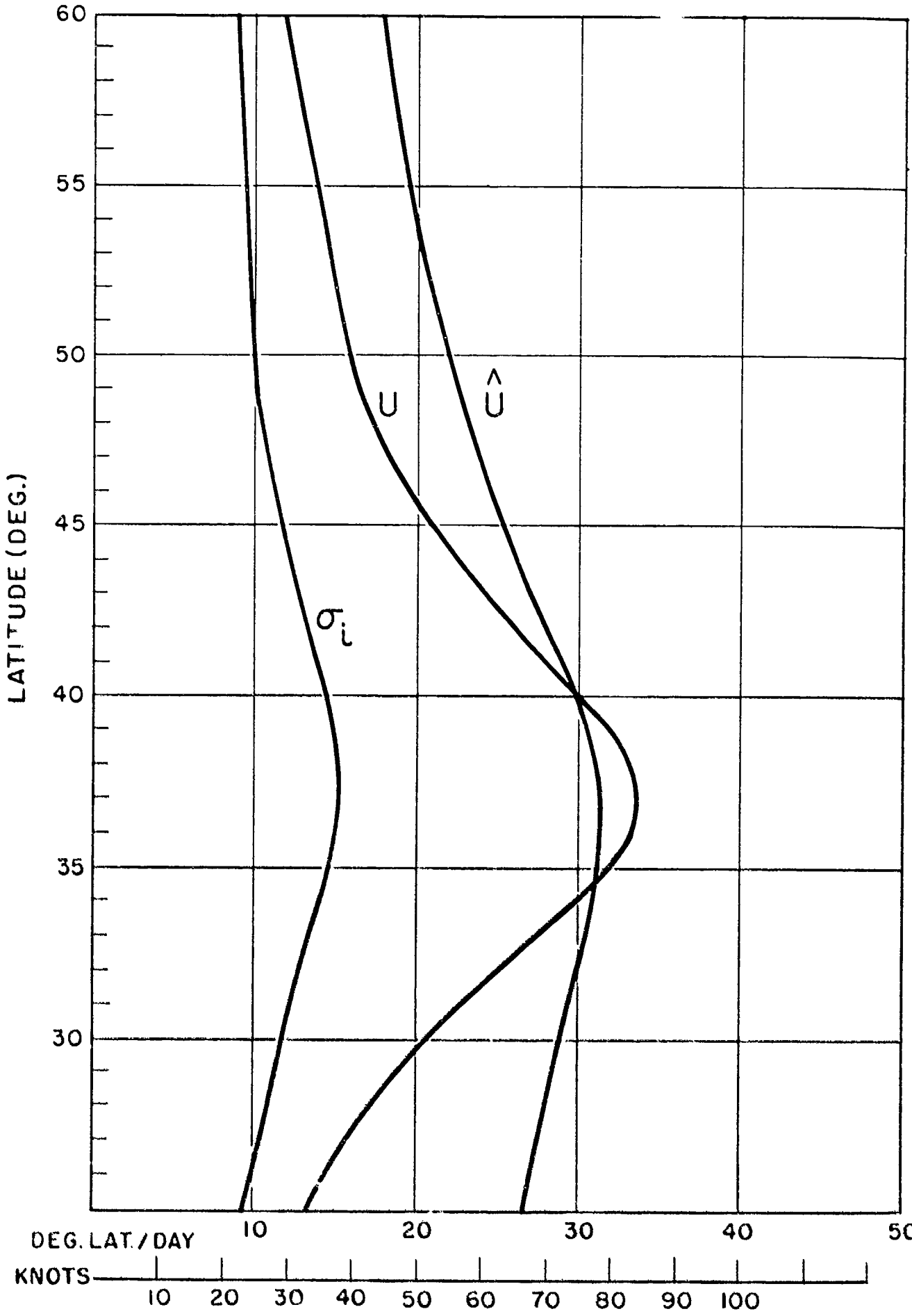

Figure 2. Mean wind and standard deviation, North America, January, 50,000 Feet

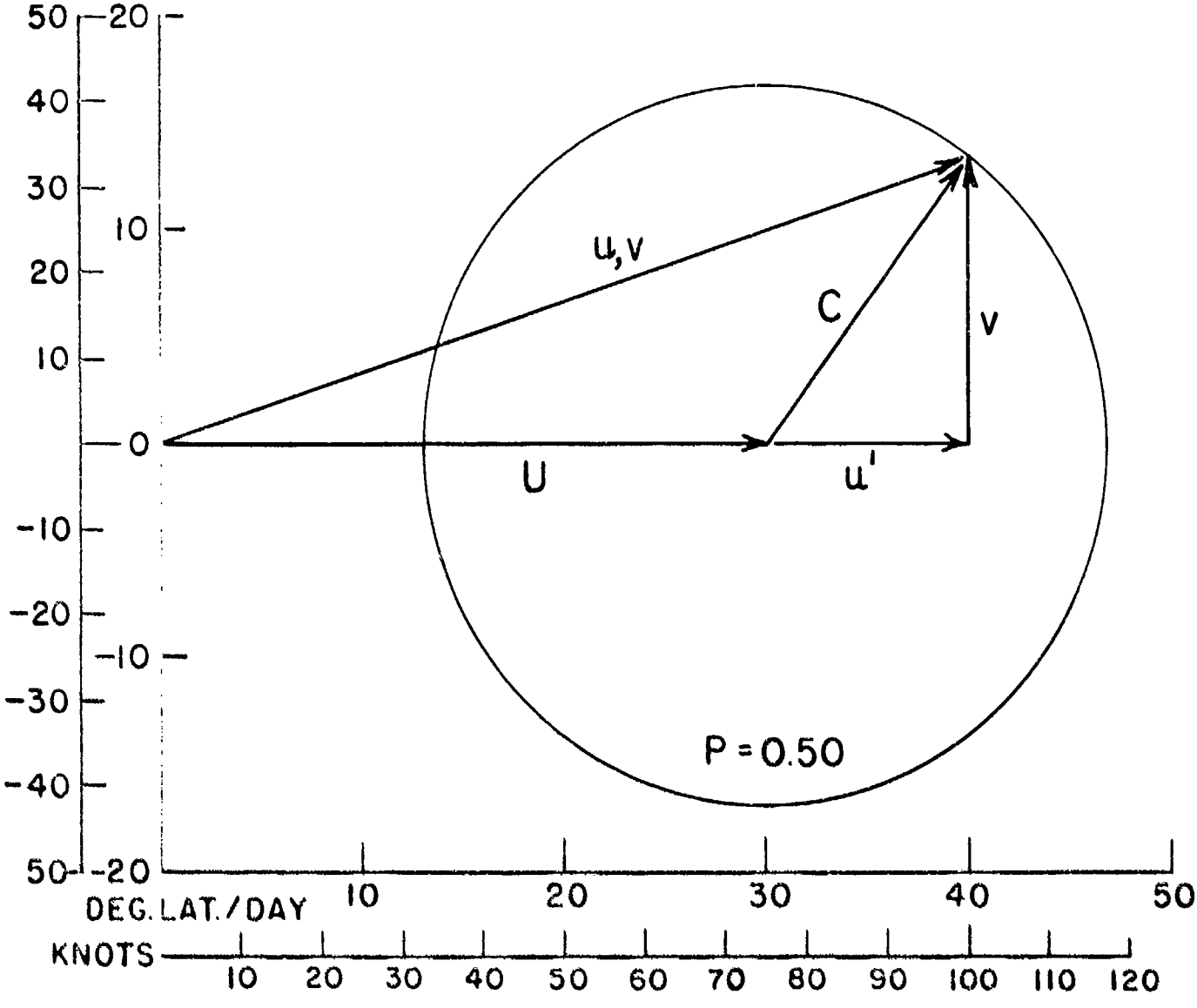

Figure 3. Circular normal distribution of winds, North America, January, 50,000 Feet, 40°N

For reasons which will become apparent later, it is necessary to solve the deviation part of the problem first. Figure 4 is a solution, for 40°N latitude, of the transformation equations (Eqs. [4] and [5]) developed in Appendix IV. The radiating curves are arcs of great circles, marked off in values of s, the linear distance from the origin. Each great circle is identified by α, a spherical angle measured from an arbitrary meridian. Note that both λ' and ϕ depend α and s. Thus we may write the following symbolic relations. (Note: The actual relations are Eqs. [4] and [5] of Appendix IV.)

$$\lambda' = A\ (\alpha, s)$$
$$\phi = B\ (\alpha, s)$$

The general method of solving the deviation part of the problem consists of:

(a) Integrating Eq. (11) with respect to s along each value of α.

(b) Determining S_{α}, the appropriate value of s for P = 0.50.

(c) Finding the λ' and ϕ values corresponding to S_{α}, using Figure 4, or Eqs. (4) and (5) of Appendix IV.

Before proceeding, however, we must first decide on a method of accounting for the variation of σ with latitude. We shall, therefore, describe two different methods of solution and compare the results obtained from each for this particular problem. The first method, called the "simplified solution," is quasi-linear, while the second method or "complete solution" is non-linear. From a computational standpoint, the essential difference between the two methods is: In the simplified solution the σ profile is introduced after integration of the probability function, whereas in the complete solution the σ profile enters the problem before integration.

We now introduce the circumflex symbol (^) to denote a quantity which is averaged between the initial latitude (in this case 40°N) and latitude ϕ. It will be understood that the method of averaging is to be specified in each case.

5. SIMPLIFIED SOLUTION OF THE DISPLACEMENT DEVIATIONS

We first assume that the mean wind is everywhere the same. Integrating Eq. (11):

$$P(S) = 0.50 = \frac{1}{\hat{\sigma}^2} \int_0^S s \exp\left(-\frac{s^2}{2\hat{\sigma}^2}\right) ds = 1 - \exp\left(\frac{-S^2}{2\hat{\sigma}^2}\right) \qquad (12)$$

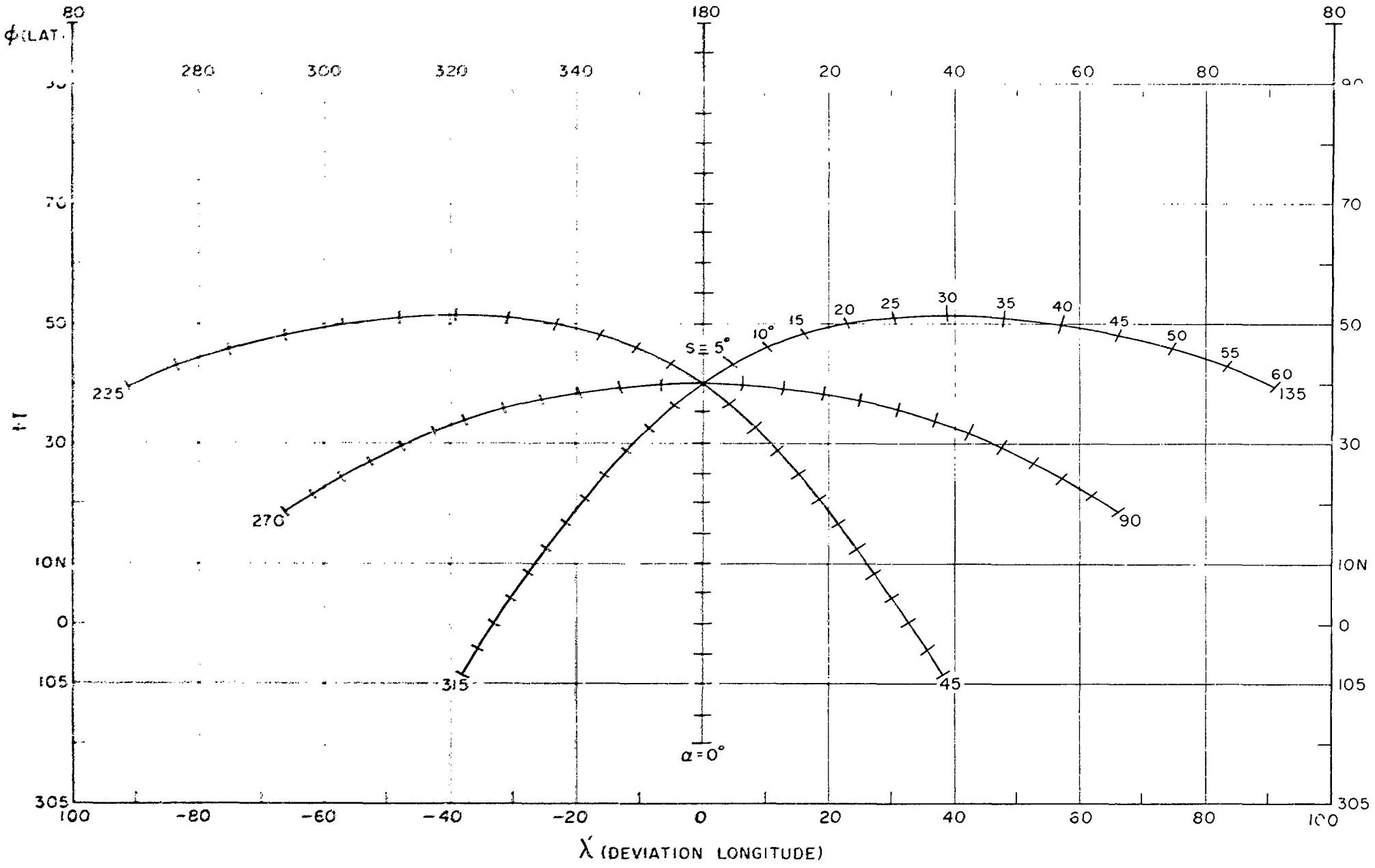

Figure 4. Solution to Eqs. (4) and (5), Appendix IV, for $0_o = 40^{\circ}N$

and

$$S = \sigma\,(\ln 4)^{1/2} = G(1)\,\sigma_i\,(\ln 4)^{1/2} \quad ,$$

and, since $G(1) = 0.86$,

$$S = 0.86 \times 1.176\,\sigma_i = 1.01\,\sigma_i \qquad (13)$$

where σ_i is expressed in degrees latitude per day. Since S is independent of α, the solution of the deviation displacements for constant mean wind is a circle on the earth's surface with a radius which is a function of U. If we compare Eqs. (13) and (13a), also Eq. (14a), we see that S is directly proportional to C. In fact, $S = 0.86C$. We have seen that C represents the radius of the wind deviation circle. However, the radius of the displacement deviation circle is not S, but $\frac{180}{\pi}\sin S$. This difference arises because the radius lies in the plane of the circle and not on the curved surface of the earth where S lies. Figure 5 is an enlargement of Figure 4 on which the deviation displacements of the 0.50 probability curve have been plotted for various values of U. Since these curves are axially symmetrical, only half of the figure is shown.

At this point we introduce the profile of U. We assume that the solution at latitude, ϕ, is the same as the solution for a constant mean wind of magnitude, $\hat{U}$, where

$$\hat{U} = \frac{\int_{40}^{\phi} U\,d\phi}{\phi - 40} \quad .$$

The profile of $\hat{U}$ is shown in Figure 2, page 11. The mapping of the 0.50 probability curve for the deviation part of the solution is shown in Figure 5.

c. COMPLETE SOLUTION OF THE DISPLACEMENT DEVIATIONS

Equation (11) is rewritten:

$$p(s) = \frac{s}{\hat{\sigma}^2}\,\exp\left[-\frac{s^2}{2\hat{\sigma}^2}\right] \quad . \qquad (11b)$$

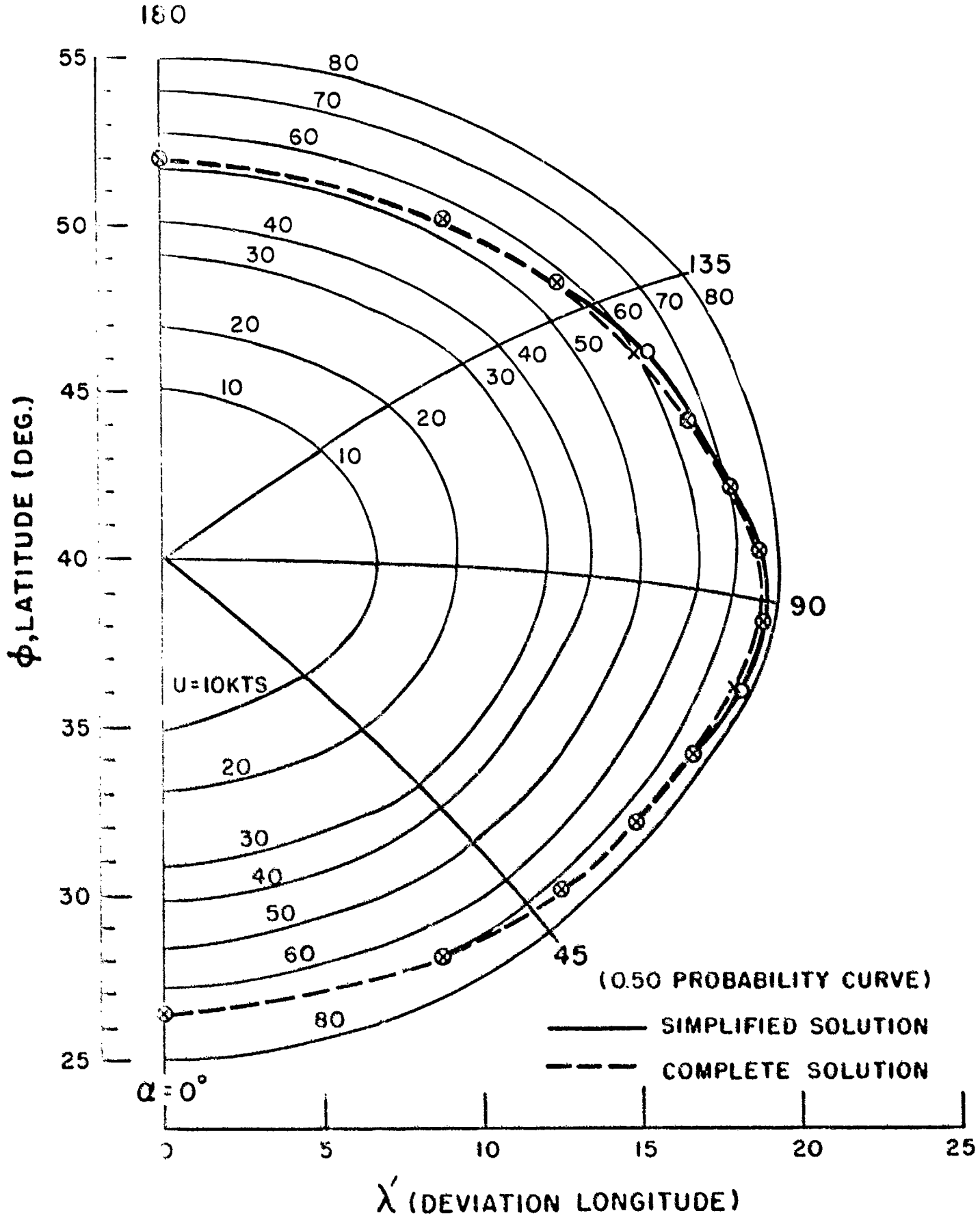

Figure 5. Solutions for the deviation displacement 0.50 probability curve

$\hat{\sigma}$ is a value of σ appropriate for the population of displacement deviations from 0 to S. Within the integration, $\hat{\sigma}$ is a constant.* Integrating Eq. (11b):

$$P(a,S) = \left[\frac{1}{\hat{\sigma}^2} \int_0^S s \exp\left[-\frac{s^2}{2\hat{\sigma}^2} \right] ds \right]_a$$

$$= \left[1 - \exp\left[-\frac{S^2}{2\hat{\sigma}^2} \right] \right]_a \qquad (12b)$$

$$S_a = \left[\hat{\sigma} \, (\ln 4)^{1/2} \right]_a = \left[G(1) \, \hat{\sigma}_i \, (\ln 4)^{1/2} \right]_a \qquad (13b)$$

$$S_a = \left[1.01 \, \hat{\sigma}_i \right]_a \, . \qquad (14b)$$

We define $\hat{\sigma}_i = \int_0^S \sigma_i \, ds/S$.

In general, $\hat{\sigma}_i$ will vary with a. Thus, unlike the solution for a constant mean wind, the complete solution is not circular.

---

* The reason for this stems from the definition of a probability distribution function. To show this, we will integrate Eq. (11) in a straightforward manner, considering $\sigma = \sigma(s)$:

$$P(S) = \int_0^S \frac{s}{\sigma^2} \exp -\left(\frac{s^2}{2\sigma^2}\right) ds \, .$$

Integrating by parts:

$$P(S) = 1 - \exp\left[-\frac{S^2}{2\sigma^2} \right] + \int_{\sigma_0}^{\sigma_S} \frac{s^2}{\sigma^3} \exp\left[-\frac{s^2}{2\sigma^2} \right] d\sigma \, .$$

As $S \to \infty$,

$$P(S) \to 1 + \int_{\sigma_0}^{\sigma_S} \frac{s^2}{\sigma^3} \exp\left[-\frac{s^2}{2\sigma^2} \right] d\sigma \, .$$

By definition, P = 1 at S = ∞ ; but, in general, the integral term on the right does not vanish. Therefore, the above equation is not a probability function.

Table 3 shows the results for this example, obtained by numerical integration.

Table 3. Computation of displacement deviation (complete solution)

DEGREES LONGITUDE, ROTATED SYSTEM		DEGREES LATITUDE		DEGREES LONGITUDE
a	$\hat{\sigma}_i$	S	$\emptyset$	λ'
0	13.33	13.46	26.5	32.5
45	14.08	14.22	29.4	36.2
90	14.61	14.76	38.5	40.2
135	12.40	12.52	47.4	32.2
180	11.65	11.87	51.9	30.0
225	12.39	12.52	47.4	-32.2
270	24.61	14.76	38.5	-40.2
315	14.08	14.22	29.4	-36.2

The solution is plotted in Figure 5. The difference in results from the two methods for the deviation part of the solution is practically negligible.

7. SOLUTION OF THE MEAN DISPLACEMENT

The mean longitude displacement for a particle moving along a latitude circle with the speed of the mean wind for that latitude is

$$\lambda = (U \sec \emptyset)\, T .$$

In the complete solution, where we consider displacements along great circles, a,

$$\lambda = (U \sec \emptyset)_a \, T \tag{15b}$$

where

$$(U \sec \emptyset)_a = \left. \int_0^{S_a} (U \sec \emptyset)\, ds \right|_a$$
$$S_a$$

In the simplified solution,

$$\Lambda = \hat{U}\,\widehat{(\sec\phi)}_a\,T \tag{16b}$$

where again $\hat{U} = \dfrac{\int_{40}^{\phi} U\,d\phi}{\phi - 40}$ and $\widehat{(\sec\phi)}_a = \dfrac{\int_{o}^{S_a} \sec\phi\,ds}{S_a}$.

The two solutions are plotted in Figure 6. It now remains to add the two parts of the solution. The final results are shown in Figure 7. It may be seen that the difference between the two solutions is quite small. Nearly all of the difference is produced by errors in the simplified solution of the mean displacement. Since the mean displacement is proportional to time, there will be a tendency for the errors to increase with time. On the other hand, the fact that S_a also increases with time will tend to diminish the errors. On the whole, it may be said that the simplified solution yields a good approximation.

8. MAPPING OF THE PROBABILITY FIELD

To illustrate the nature of the probability field, we have plotted probability maps for an initial point of 40°N and 120°W at 50,000 feet for January and July, and for time periods of 1, 2, and 3 days (Figures 8 through 13). The computation method used to obtain this series of charts was precisely the same as outlined for the complete solution. These maps may be interpreted or used in several ways. As a simple example, suppose that a constant-level balloon is launched at 50,000 feet in January from the initial point. If we have no further information, then the indicated probability gives the correct odds that the balloon will be located within the area enclosed by the given probability curve after t days. Thus, the probability is 0.25 that the balloon is within the 0.25 curve versus 0.75 that it is outside. Similarly, the probability is 0.99 that the balloon is within the 0.99 curve versus 0.01 that it lies outside. The most probable area is enclosed by the 0.50 probability curve.

With suitable refinements, this presentation could possibly be used for problems involving atomic fallout. In this case, we would need distribution functions at several atmospheric levels. We cannot, of course, provide detailed

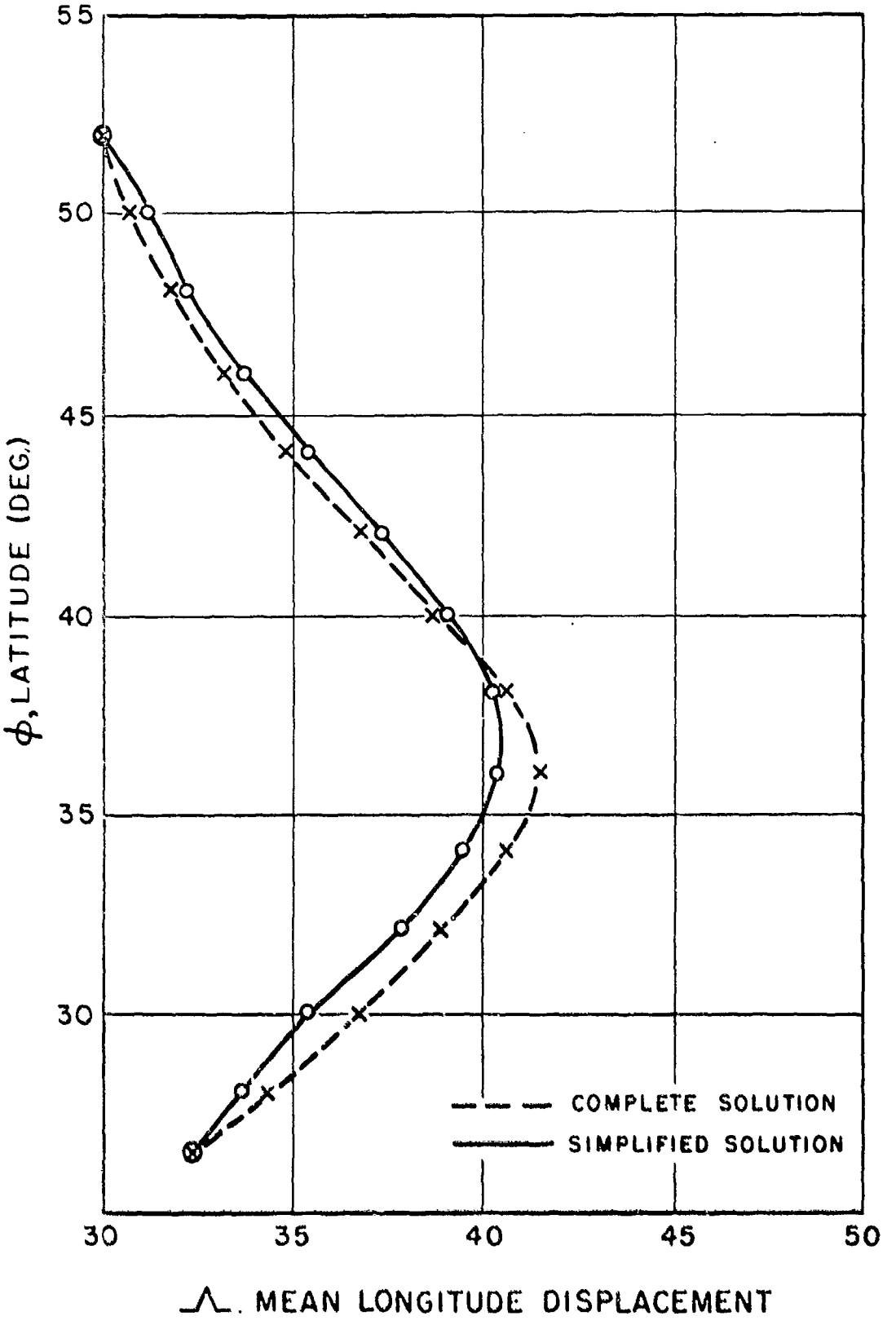

Figure 6. The solution for the mean displacement

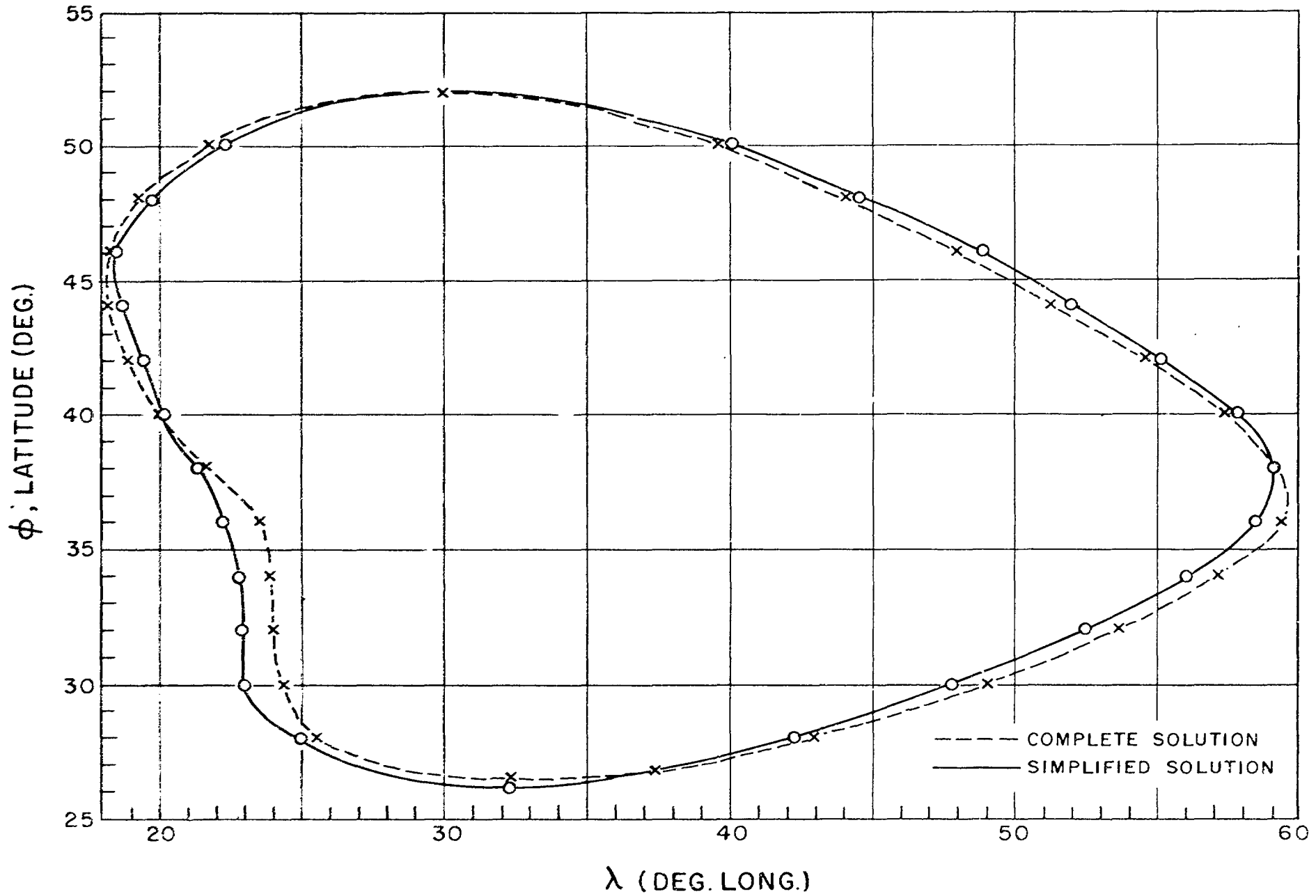

Figure 7. Mapping of the final solution for $t_1 = 0.50$ and $h_1 =$

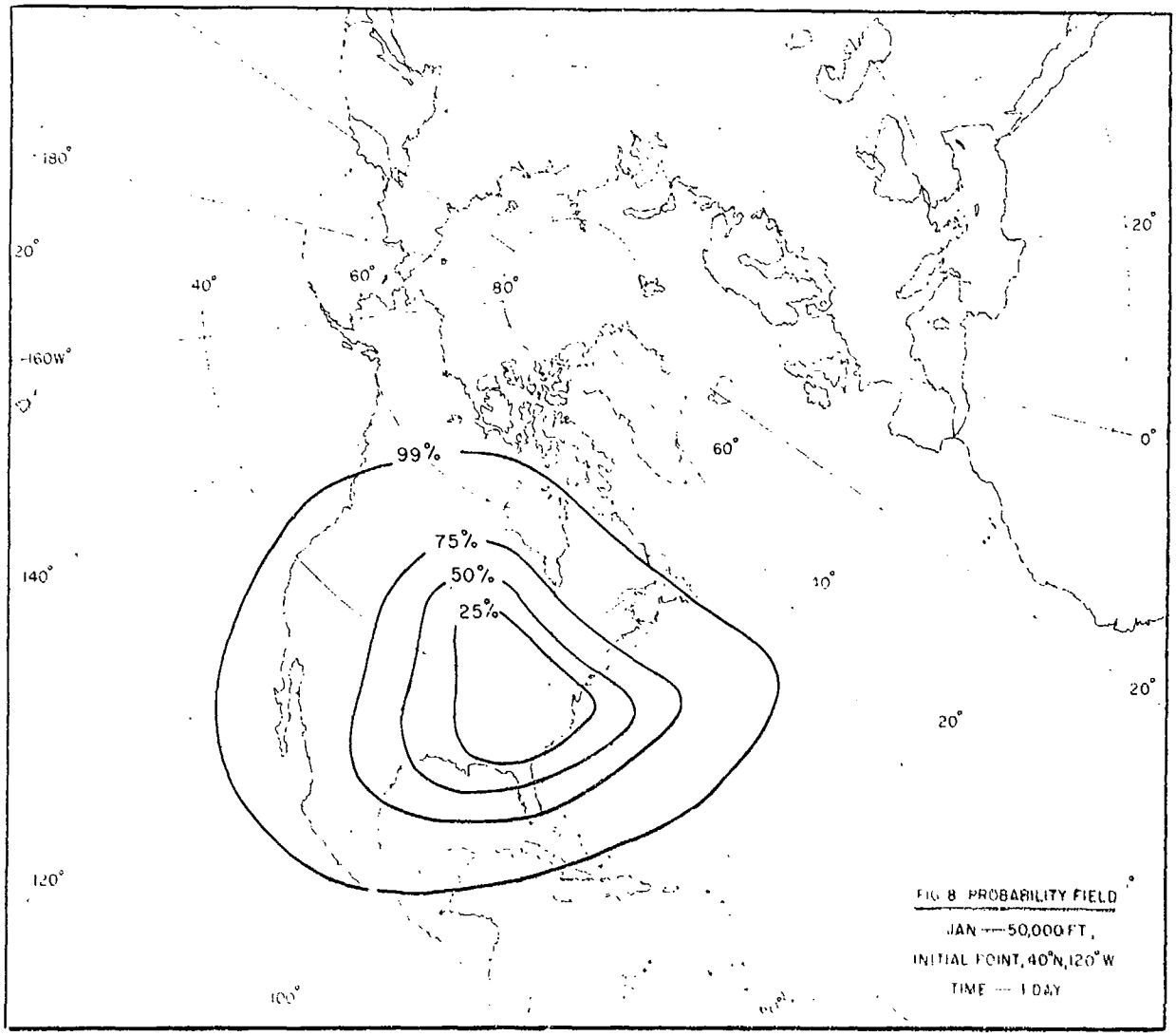

Figure 8. Probability field, January, 50,000 Feet; initial point, 40°N, 120°W; time, 1 day

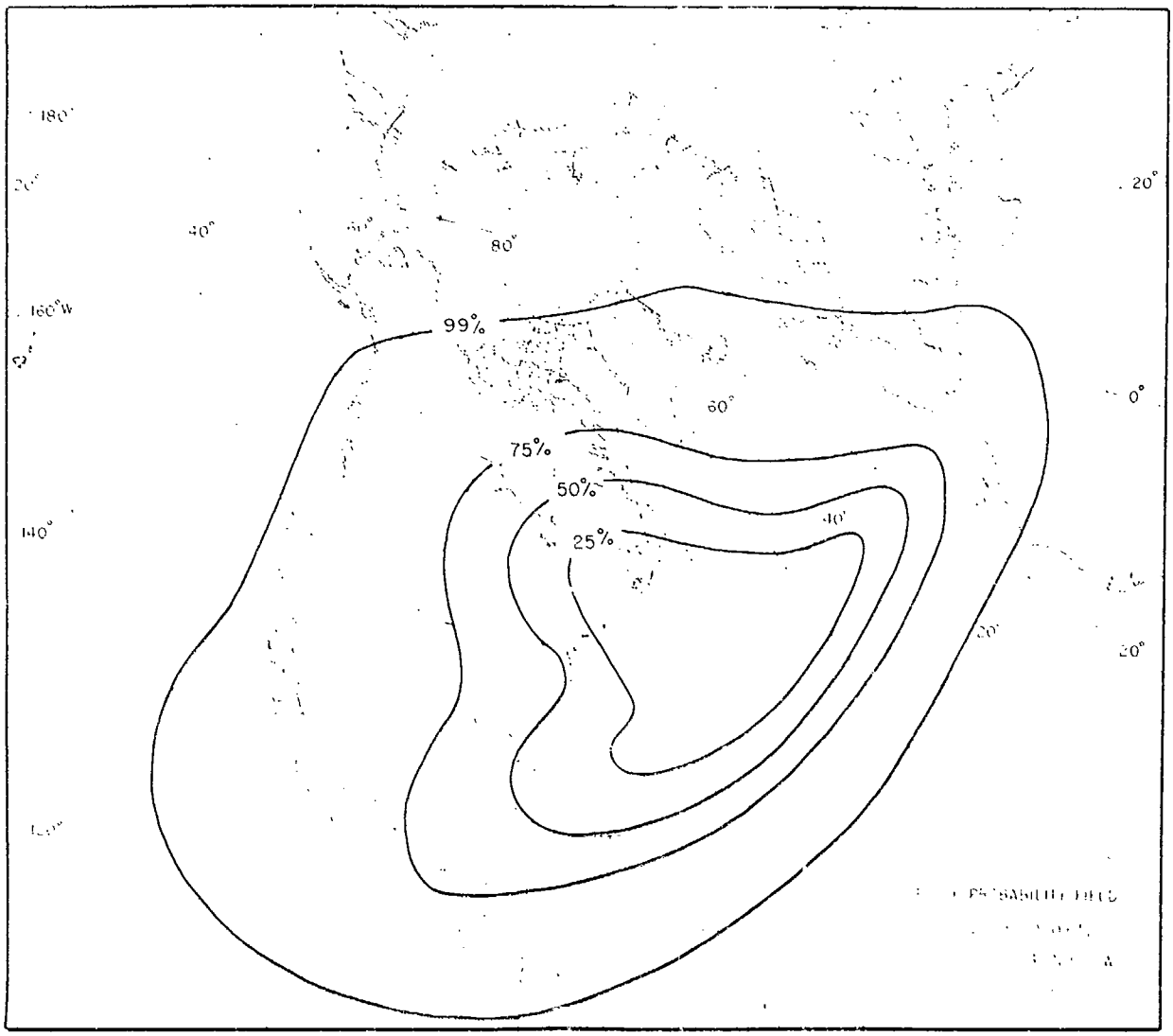

Figure 9. Probability field, January, 50,000 Feet; initial point, 40°N, 120°W; time, 2 days

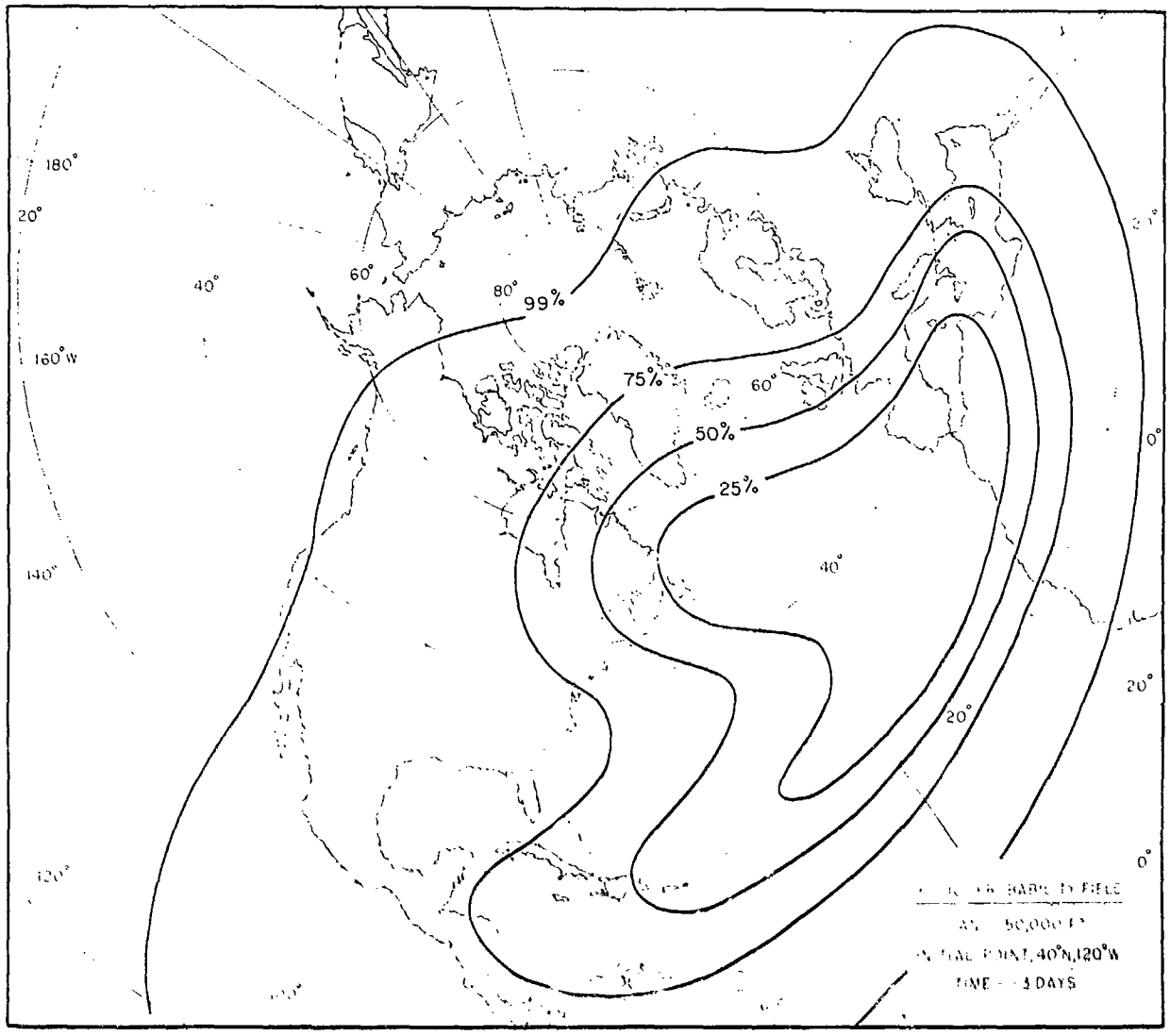

Figure 10. Probability field, January, 50,000 Feet; initial point, 40°N, 120°W; time, 3 days

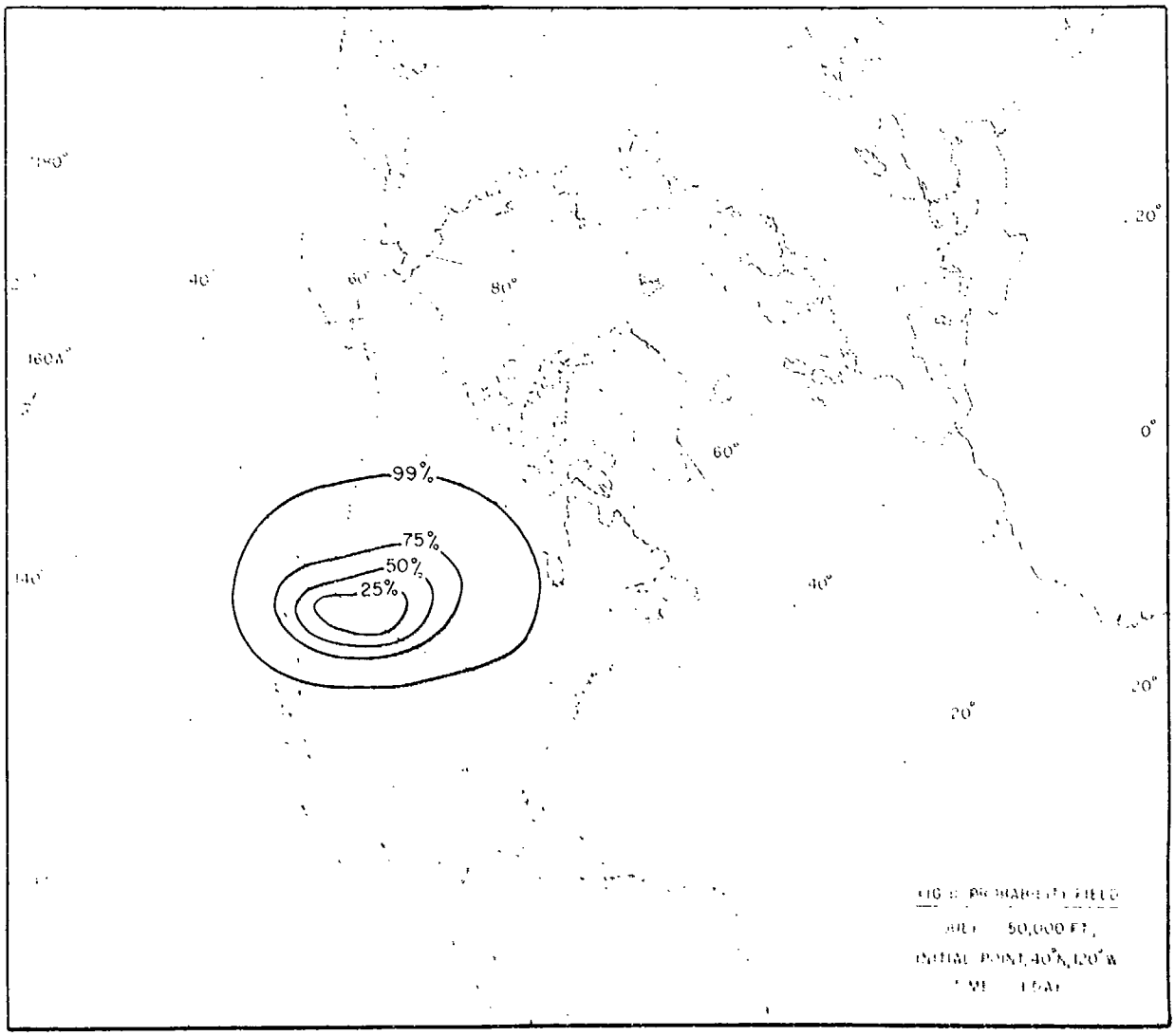

Figure 11. Probability field, July, 50,000 Feet; initial point, 40°N, 120°W; time, 1 day

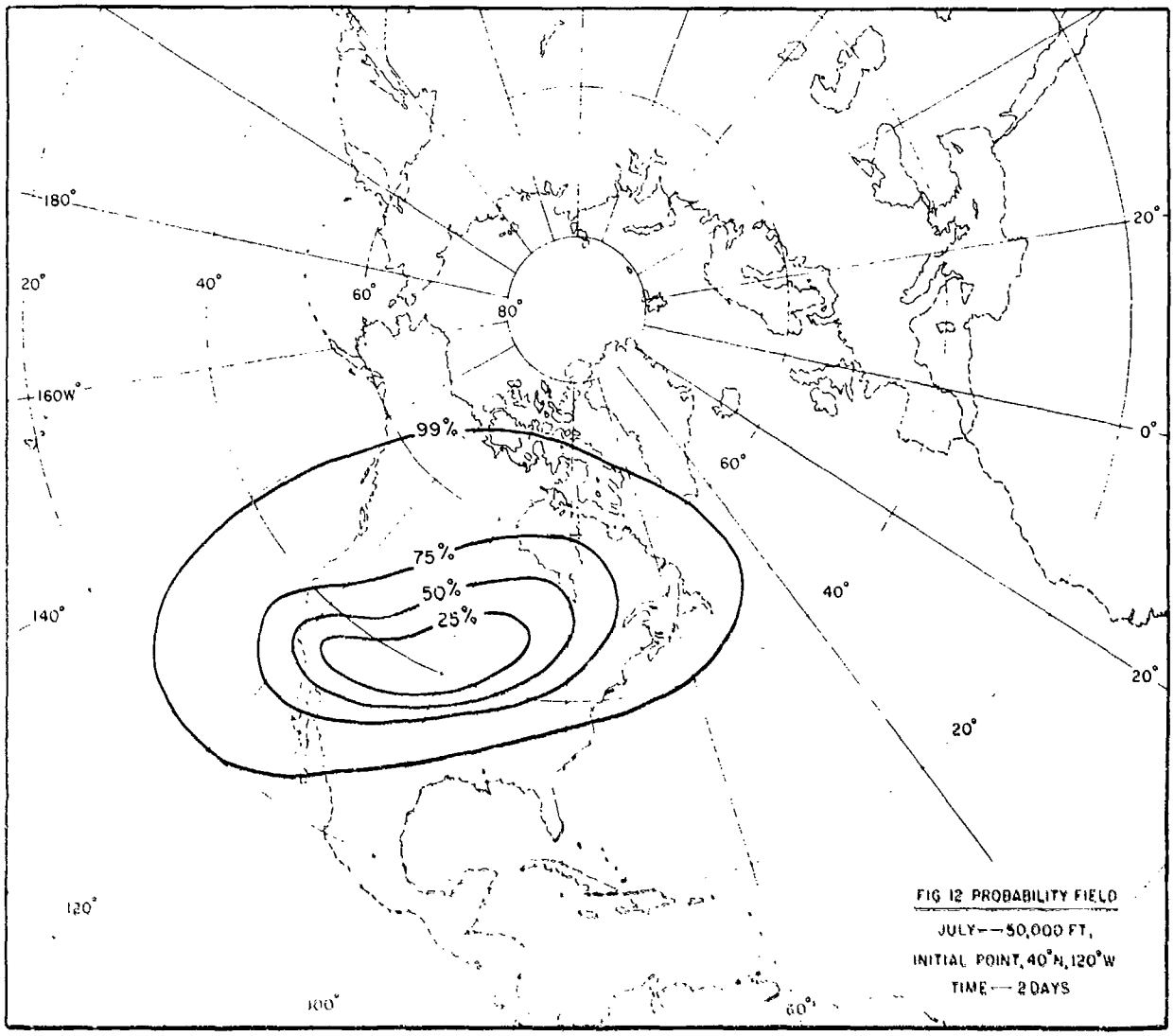

Figure 12. Probability field, July, 50,000 Feet; initial point, 40°N, 120°W; time, 2 days

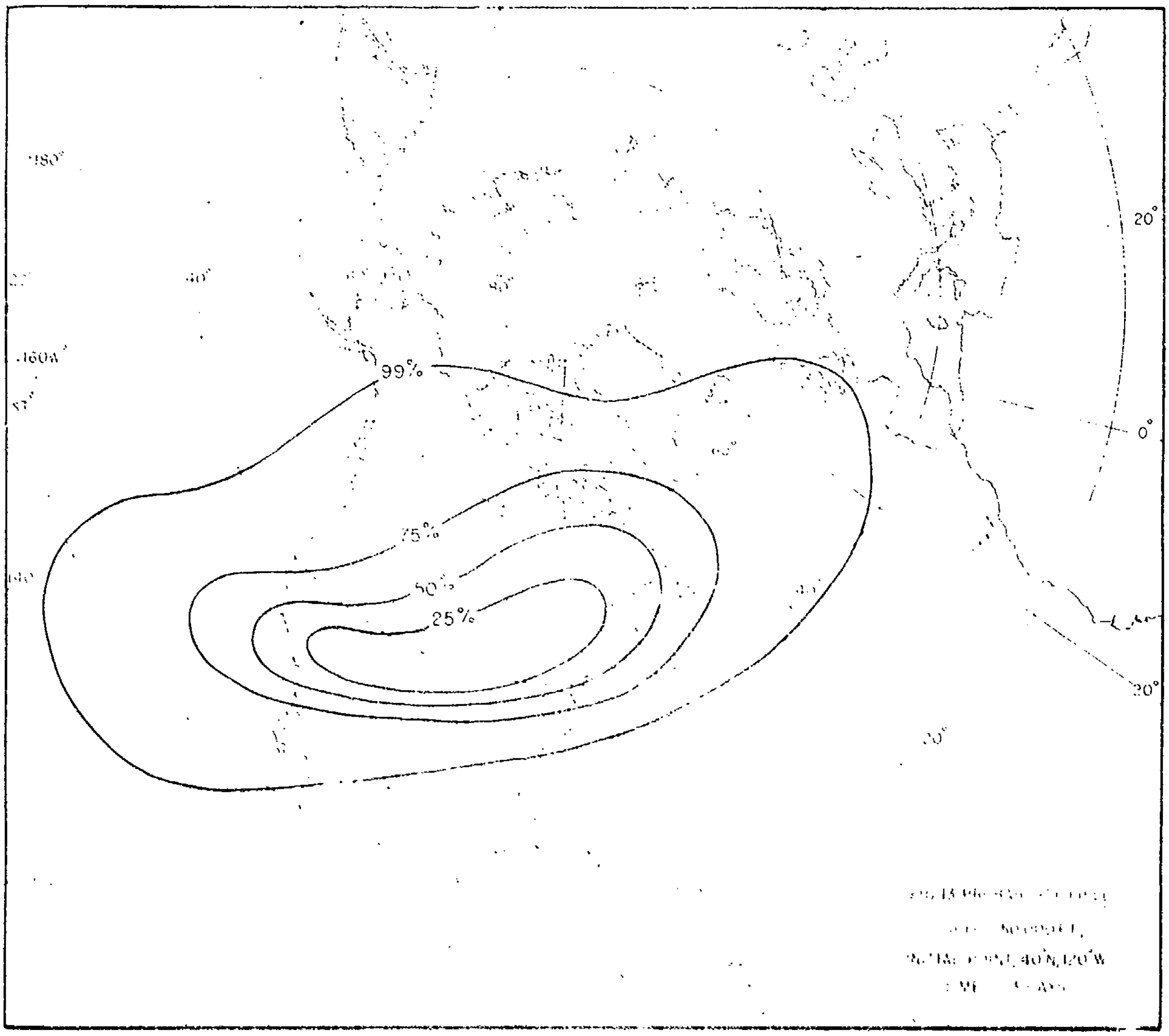

Figure 13. Probability field, ... feet; ... 40°N, 120°W; time, 3 days

information on the amount of concentration since this is a small-scale phenomena. However, we can provide information on the location of high concentration areas.

The foregoing probability statements were made with the understanding that our only available information is the time and place of the balloon launching. Now, suppose that we are given one further bit of information, namely, the initial wind velocity. Our theory permits us to construct a different set of probability maps which take into account this information. In the first few days, the areas enclosing the probability curves would be smaller and the central path would be different. With the passage of time, differences between the two sets of maps would tend to disappear. In other words, the added information reduces some of the uncertainty about the balloon's location, but the information becomes less important with increasing time.

9. THE DOWNSTREAM PROBABILITY FUNCTION

For balloon operations, the most useful probability statement is the "Downstream Probability Density Function" (DPDF). This may be defined as the probability density with respect to latitude of an x-displacement at least as large as a specified value and occurring within T days. Mathematically, this density function is expressed as follows:

$$\mathrm{DPDF} = \int_0^T p_{y,t} \frac{\partial}{\partial t}\left(1 - P_{x,t}\right) dt \,. \tag{17}$$

If we wish to interpret this function in terms of balloon operations, we first assume that a large number of balloons are launched from a single point over a long period of time. In this case, x and y are components measured from the launching site and t refers to the time interval after launching. The term $(1 - P_{x,t})$ represents the proportional number of balloons to be found downstream from x at time t; $\frac{\partial}{\partial t}(1 - P_{x,t})$ represents the rate at which balloons flow past x at time t, $p_{y,t} \frac{\partial}{\partial t}(1 - P_{x,t})$ represents the rate at which balloons flow downstream past the point x, y at time t. Finally, Eq. (17) represents the proportional number of balloons which may be expected to have

flowed downstream past the point x, y from the time of launching to the time T.

The various steps in the computations required to solve Eq. (17) for a specific example are illustrated in Figure 14. For convenience, we substitute for $p_{y,t}$ the probability for a small increment of y, namely, $\Delta p_{y,t} = (P_{y+\Delta y} - P_y)_t$.

The DPDF must be mapped on a spherical earth and the variation of δ and U with latitude must be taken into account, just as in the case of the polar integration. It has been previously demonstrated that use of the simplified solution introduces very little error into the results. For this reason it was decided to adopt the simplified solution for computing the DPDF. Accordingly, Eq. (17) was solved for various values of U, s, y, and t. The next step is to eliminate x by the transformation, $\lambda = x \sec \phi$. For y we substitute $\phi - \phi_o$. We now have a table with the parameters, U, ϕ_o, λ, and ϕ. This is Table I, Volume II. The final step is to substitute the values of $\hat{U}$ for U for each region, season, and height. Here again

$$\hat{U} = \frac{\int_{\phi_o}^{\phi_s} U \, d\phi}{\phi_s - \phi_o}$$

We now have a set of tables for each region, season, and height for various values of ϕ_s, λ, and ϕ. Two such tables appear in Volume III, namely, Table I, North America, and Table II, Eurasia.

There are two limitations on the downstream probability concept. In the first place, on a spherical earth some air particles may take a decided northward course and reappear at a lower latitude very far downstream. While it would be feasible to formulate a solution which incorporates this type of trajectory, we decided to exclude these cases from consideration. Thus the computations in Volumes II and III refer only to those motions which are essentially downstream.

The second limitation occurs when the mean zonal wind changes sign at some latitude. This occurs, for example, over North America at 60,000 feet in summer and at 80,000 feet in the fall for certain initial latitudes. Our solution here is to make two sets of tables, one for eastward displacements and the other for westward displacements.

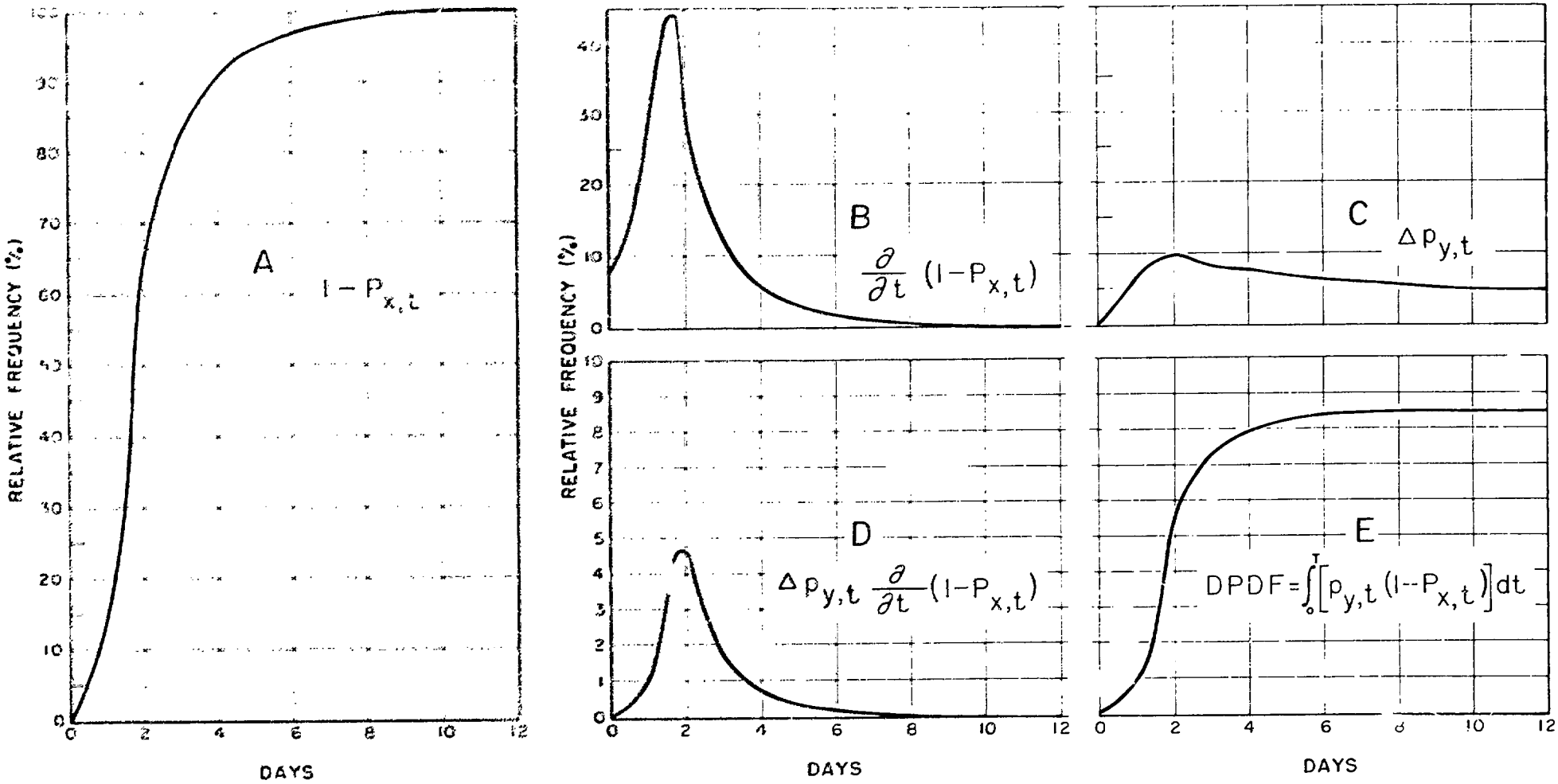

Figure 14. Example of the downstream probability computation for: x = 20° latitude; y = 10° to 15°N; U = 30 knots

APPENDIX I

WIND ANALYSIS

To obtain a complete solution of the wind climatology problem, certain basic quantities must be plugged into the statistical equations. These include the variation by season, latitude, and height of the mean instantaneous wind and its associated distribution functions. This is analogous to the solution to a vast jigsaw puzzle where many important pieces are missing.

The first step in the solution was a rather complete survey of available literature. From this we were able to deduce a somewhat sketchy broad-scale picture of the wind distribution at upper levels over the earth. It became immediately apparent that for more details we would have to resort to indirect or "bootstrap" techniques.

One of the desired quantities is some measure of the distribution associated with the mean wind. If the wind is normally distributed, a single parameter, such as the standard vector deviation or the constancy (ratio between the vector mean wind and the scalar mean wind), can be used.[3] For convenience and ease of computation, it was decided to compute the wind constancy. To minimize the known bias in the observed upper wind records, the difference method of averaging[7] was used throughout the study.

We decided to concentrate on an intensive analysis of three data sources: (a) a 9-year record of 15 U. S. Weather Bureau Stations; (b) a series of 3 to 4 years of upper air synoptic maps of the West German Meteorological Service[8] at 3 levels: 500 mb (20,000 ft), 225 mb (36,000 ft) and 96 mb (54,000 ft); and (c) rawinsonde records from Berlin and several other German stations.

Each of the German synoptic charts for the months of January, April, July and October was photographically enlarged to a size of 15" by 20", and isotachs (lines of equal wind speed) were constructed, using the computed geostrophic winds as well as observed wind speeds. From the analyzed charts, mean vector and scalar winds were computed for each latitude, season, and height, combining the data from longitude 30°W to 30°E into a single statistic.

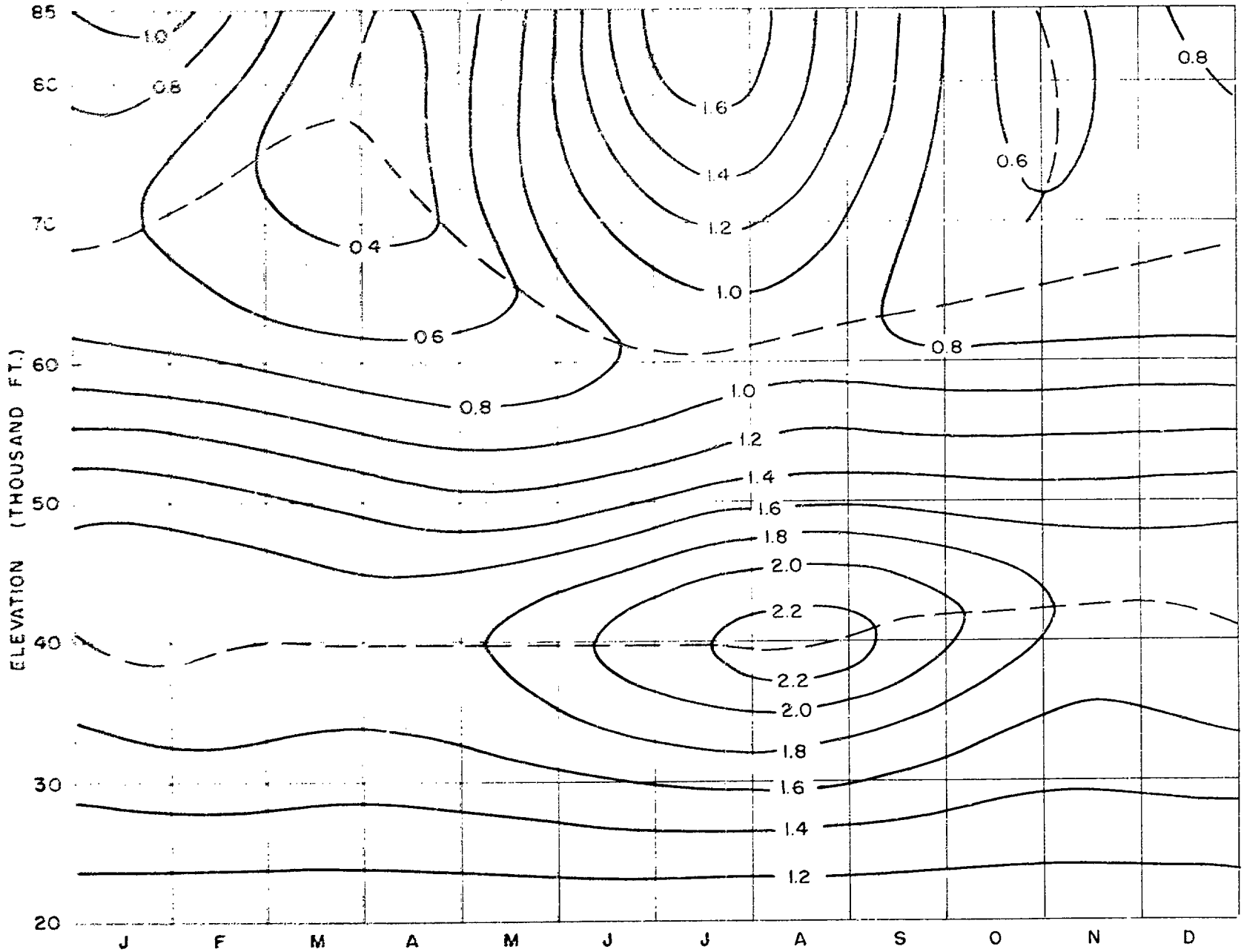

Figure 15. Ratio of wind speed at any level to the speed at 6 km (20,000 ft), average for 5 United States' stations (approximately 37°N)

In all, 1000 maps were analyzed and 35 wind values computed from each map.

The United States data were summarized by punched cards. The ratio between the scalar winds at any level and some standard level was the most stable statistic that could be found. For this reason all the data were reduced to ratios between the scalar wind speeds at given levels and the corresponding scalar winds at 6 kilometers. Summarized values of this statistic were smoothed by harmonic analysis and matched, level for level, with similar data from European sources. In this way the latitudinal variation of the scalar ratio was established. For levels above 96 mb the German wind data were used in the comparison. These were supplemented by data from manuscript Northern Hemisphere synoptic maps for 1953 at 100 mb (53,000 ft) and 50 mb (68,000 ft). Figure 15 is an example of one set of ratio analysis. The trough lines in the upper portion of the chart delineate the boundaries of the easterlies.

Having established the scalar wind ratios, it was then possible to compute reliable scalar wind speeds by multiplying the ratios with the appropriate mean scalar winds at 500 mb which are known with considerable accuracy.

This left the vector mean winds to be determined. It was found that this statistic was difficult to determine accurately from a limited sample because of variations in wind direction. An intensive study of the 500-mb United States data led to the discovery that a remarkably consistent relationship existed between the scalar and vector mean winds. It is well known that strong winds are more constant than weak winds. Since the ratio between the vector and scalar wind is a measure of wind constancy, this ratio should rise as the wind increases. This was found to be the case. It was also found that the presence of the mean Jet Stream produces an additional increase in constancy over and above the effect of wind speed alone. This effect is also known qualitatively. These relationships are shown in Figure 16. The degree to which the United States 500-mb data fitted the derived curves suggested the possibility that this was a universal statistical law governing the westerlies. Attempting to verify this suggestion stringently, we used test data from a distant region, a remote level, and for a different time period, namely, the 96-mb wind data for Europe. Table 4 shows the excellent results of this test. Consequently, we may conclude

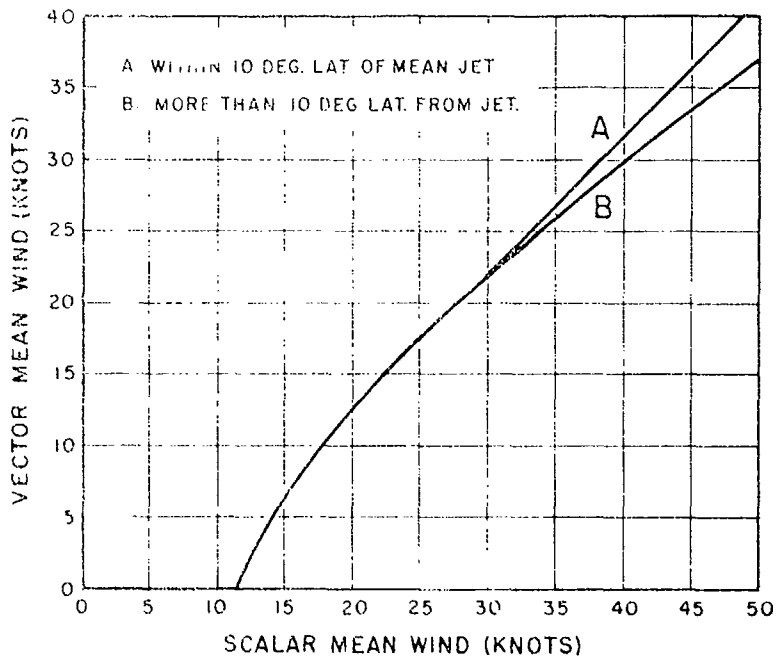

Figure 16. Relation between scalar wind and vector wind in westerlies

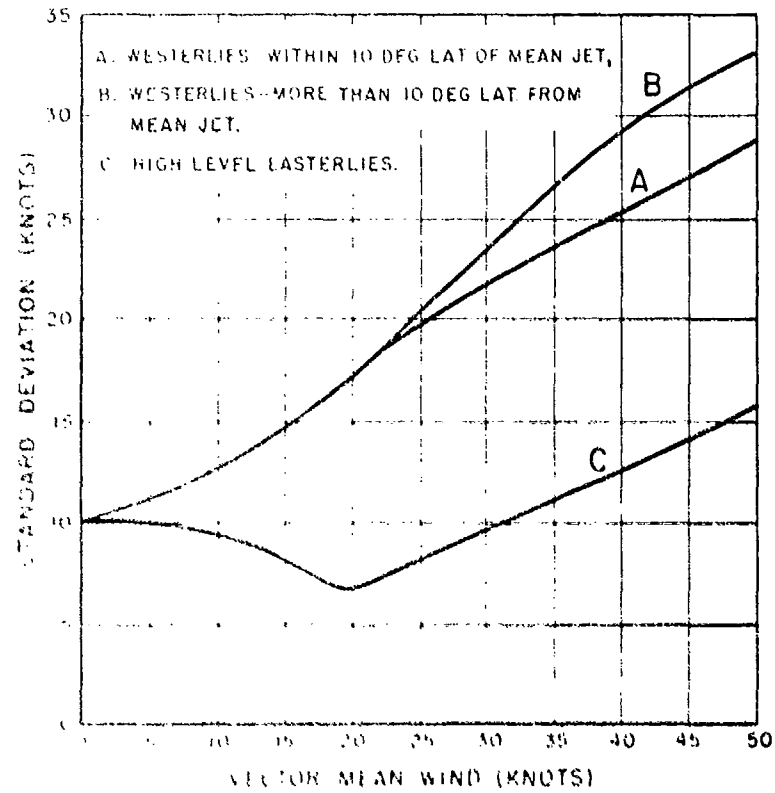

Figure 17. [illegible] wind and standard vector deviation

that the mean wind uniquely determines its distribution function.

Table 4. Correlation of test data (96-mb winds (kts) over Europe)

MONTH	LATITUDE	SCALAR WIND	VECTOR WIND	
			Predicted	Observed
Jan	70	37.0	27.2	26.9
Jan	60	46.3	37.4	36.9
Jan	50	37.4	27.5	26.9
Jan	40	37.6	27.6	27.0
Jan	35	40.9	32.1	31.3
Apr	70	27.3	19.3	17.1
Apr	60	28.8	20.6	21.4
Apr	50	22.9	15.3	13.4
Apr	40	29.0	20.7	19.9
Apr	35	35.7	27.0	28.3
Jul	70	16.9	8.5	7.0
Jul	60	20.0	12.4	11.6
Jul	50	20.6	13.0	11.0
Jul	40	24.8	17.2	16.7
Jul	35	26.8	18.9	21.0
Oct	70	27.5	19.5	19.8
Oct	60	28.6	20.4	19.8
Oct	50	25.3	17.6	16.0
Oct	40	27.5	19.5	18.0
Oct	35	29.7	21.2	21.9

Correlation coefficient, $r = 0.99$

A similar relationship was derived for the easterlies from what little data were available. Considerably less confidence can be placed in these results. Nevertheless, indications are that the high-level easterlies are extremely constant winds.

Using the data from Figure 16 we computed the relation between the vector mean wind and the standard deviation (Figure 17).

APPENDIX II

UPPER WINDS OVER EUROPE AND NORTH AMERICA

The mean zonal winds and standard deviations used in this study are presented in Table 5. Above 54,000 feet the sparse European data was supplemented by more complete data from North America. Thus the winds at high levels in Europe, while not as reliable as the lower winds, may be regarded as a first approximation to the true winds. The standard deviations in Table 5 are taken from Figure 17, Appendix I.

Figures 18 through 23 summarize the important variations of the winds in Table 5, namely, seasonal, latitudinal, and vertical. The 80,000-foot curves are typical for the region above 50,000 feet. The 40,000-foot curves are characteristic of the layer below 50,000 feet.

1. SEASONAL VARIATION (Figures 18 and 19)

The seasonal variation of winds at 40,000 and 80,000 feet over North America at 40°N (Figure 18) and Europe at 50°N (Figure 19) was obtained by harmonic analysis. Over both regions a single wave was sufficient to represent the 80,000-foot data while two waves were required to fit the 40,000-foot winds.

The 80,000-foot seasonal variation for both continents consists of a single maximum of westerlies in midwinter and a single maximum of easterlies in midsummer with reversals of direction in April and September.

At 40,000 feet the double-wave structure in the westerlies is very pronounced in Europe and quite small in North America. There are two distinct maxima in Europe, the primary in March and the secondary in November; and two minima, the major in August and minor in February. By contrast, the North American curves show a very pronounced maximum of 100 kts in January and a mere suggestion of a secondary maximum in July. The effect of the second wave in this case is to flatten out the summer minimum (that is, easterly maximum) so that the mean zonal wind is virtually constant from May

	NORTH AMERICA										EUROPE							
	40,000		50,000		60,000		70,000		80,000		40,000		50,000		60,000		70,000		80,000	
ℓ	u	σ	u	σ	u	σ	u	σ	u	σ	u	σ	u	σ	u	σ	u	σ	u	σ
											JANUARY									
75		[illegible]	15	13.4	[illegible]	22.8	44	26.5	80	36.9	21	17.7	22	18.3	19	16.5	20	17.1	20	17.1
70	7	[illegible]	22	19.6	[illegible]	25.2	64	32.7	80	36.9	26	20.8	27	21.4	22	18.3	23	18.9	24	19.5
65	26	[illegible]	30	22.8	33	23.5	58	24.7	43	26.9	38	24.7	33	23.5	25	20.2	24	19.5	27	21.4
60	32	26.2	39	23.8	26	22.0	28	22.0	31	23.0	42	25.8	36	24.2	26	20.8	25	20.2	28	22.0
55	36	24.7	36	24.0	32	23.2	29	22.4	26	20.8	40	25.2	35	24.0	25	20.2	24	19.5	27	21.4
50	45	27.4	40	25.2	36	24.2	31	23.0	24	19.5	37	24.4	30	22.8	21	17.7	22	18.3	25	20.2
45	78	36.5	63	29.8	38	24.7	32	23.2	26	20.8	36	24.2	28	22.0	18	16.0	19	16.5	21	17.7
40	109	41.3	79	33.8	45	26.4	35	24.0	30	22.8	36	24.2	29	22.4	18	16.0	16	15.0	18	16.0
35	87	36.2	80	33.9	50	26.6	36	24.2	30	22.8	45	26.9	36	24.2	21	17.7	14	14.1	16	15.0
30	58	31.0	52	29.2	37	24.4	22	18.3	14	14.1	46	27.2	39	24.9	23	18.9	13	13.7	15	14.6
25	47	30.7	35	26.9	19	18.4	0	10.0	-12	8.9	44	26.5	36	24.2	21	17.7	12	13.4	15	14.6
											APRIL									
75	9	12.3	3	10.7	0	10.0	0	10.0	0	10.0	21	17.7	15	14.6	8	12.0	1	10.2	-6	9.8
70	9	12.3	5	11.2	9	12.3	12	13.4	9	12.3	28	22.0	20	17.1	9	12.3	-1	10.0	-5	9.9
65	9	12.3	7	11.7	9	12.3	11	12.6	4	11.0	46	27.2	27	21.4	9	12.3	-2	10.0	-4	10.0
60	18	16.0	12	13.4	8	12.0	7	11.7	1	10.2	51	28.9	30	22.8	9	12.3	-3	10.0	-4	10.0
55	33	23.5	23	18.9	14	14.1	8	12.0	2	10.5	49	28.3	30	22.8	8	12.0	-3	10.0	-4	10.0
50	46	26.2	32	23.2	20	17.1	10	12.6	4	11.0	46	27.2	25	22.0	6	11.4	-4	10.0	-6	9.8
45	45	26.2	32	23.2	19	16.5	6	11.4	2	10.5	42	25.8	26	20.8	6	11.4	-5	9.9	-8	9.6
40	47	26.5	42	25.8	25	18.9	0	10.0	-5	9.9	41	25.4	26	20.8	7	11.7	-6	9.8	-9	9.5
35	62	32.2	50	28.6	31	23.0	15	14.6	5	11.2	48	27.9	32	23.2	11	13.0	-7	9.7	-9	9.5
30	58	31.0	50	28.6	25	20.2	5	11.2	-5	9.9	50	28.6	35	24.0	12	13.4	-8	9.6	-8	9.6
25	61	31.9	44	26.5	16	15.0	-5	9.9	-15	8.0	48	27.9	32	23.2	11	13.0	-9	9.5	-8	9.6
											JULY									
75	-11	9.1	-16	8.8	-23	7.3	-28	8.8	-37	11.6	18	16.0	13	13.7	0	10.0	-20	6.6	-31	9.7
70	-5	9.9	-12	8.9	-16	7.6	-21	6.8	-24	7.1	22	18.3	13	13.7	-3	10.0	-24	7.6	-33	10.3
65	20	17.1	10	12.6	0	10.0	-8	9.6	-11	9.3	23	22.0	13	13.7	-6	9.8	-28	8.8	-35	11.0
60	28	22.0	20	17.1	8	12.0	-1	10.0	-10	9.3	33	23.5	13	13.7	-8	9.6	-30	9.3	-36	11.2
55	36	24.2	25	20.2	13	13.7	3	10.7	-5	9.9	33	23.5	13	13.7	-8	9.6	-30	9.3	-37	11.6
50	45	26.9	31	23.0	14	14.1	0	10.0	-6	9.8	32	23.2	13	13.7	-8	9.6	-30	9.3	-37	11.6
45	42	24.2	32	23.2	13	12.6	-5	9.9	-14	8.3	32	23.2	14	14.1	-7	9.7	-30	9.3	-37	11.6
40	26	24.2	21	17.7	4	11.0	-10	9.3	-21	6.8	34	23.7	18	16.0	-4	10.0	-29	9.0	-36	11.2
35	12	13.4	4	11.0	-4	10.0	-12	6.9	-18	6.8	42	25.8	25	20.8	0	10.0	-27	8.4	-34	10.6
30	0	10.0	-5	9.9	-12	6.9	-22	7.1	-27	8.4	44	26.5	29	22.4	1	10.2	-25	7.8	-32	10.0
25	-5	9.8	-11	9.1	-17	7.3	-26	6.8	-40	12.5	42	25.8	26	20.8	0	10.0	-23	7.3	-30	9.3
											OCTOBER									
75	7	11.7	0	10.0	0	10.0	7	11.7	8	12.0	16	15.0	15	14.6	8	12.0	1	10.2	-6	9.8
70	11	13.0	10	12.6	11	13.0	12	13.4	12	13.4	21	17.7	20	17.1	9	12.3	-1	10.0	-5	9.9
65	15	14.6	16	14.0	15	15.0	17	15.5	16	15.0	30	22.8	27	21.4	9	12.3	-2	10.0	-4	10.0
60	41	25.2	32	23.2	26	20.8	22	18.3	18	16.0	35	24.0	30	22.8	9	12.3	-3	10.0	-4	10.0
55	43	24.2	35	24.0	27	21.4	22	18.3	17	15.5	36	24.2	30	22.8	8	12.0	-3	10.0	-4	10.0
50	41	27.2	37	24.4	29	20.8	15	14.6	11	13.0	37	24.4	28	22.0	6	11.4	-4	10.0	-6	9.8
45	46	27.9	36	24.7	22	18.3	9	12.3	-7	9.7	36	24.2	26	20.8	6	11.4	-5	9.9	-8	9.6
40	48	27.9	34	23.7	19	16.5	14	14.1	10	12.6	36	24.2	26	20.8	7	11.7	-6	9.8	-9	9.5
35	51	29.9	29	25.0	13	13.7	5	11.2	0	10.0	43	26.2	32	23.2	11	13.0	-7	9.7	-9	9.5
30	37	24.4	20	17.1	0	10.0	-13	8.6	-20	6.6	46	27.2	35	24.0	12	13.4	-8	9.6	-8	9.6
25	25	20.2	10	12.6	-6	9.8	-15	8.0	-24	7.6	44	26.5	32	23.2	11	13.0	-9	9.5	-8	9.6

Table 5. Mean zonal wind, $\bar{u}$, and standard deviation, σ

through September. Note that the North American winds are more than twice as strong as the European winds in winter at the 40,000-foot level.

2. LATITUDINAL VARIATION (Figures 20 and 21)

At 40,000 feet both the winter and summer latitudinal profiles for North America each show a single, sharp maximum (Figure 20) while the corresponding curves for Europe display double maxima (Figure 21). A comparison of the January and July curves reveals that the European maxima at 60°N and 33°N remain fixed in position, whereas the single maximum over North America migrates northward from 40°N in January to 45°N in July. Note also the difference in range of the mean zonal winds with respect to latitude in North America as compared with Europe. The range is far greater in North America than in Europe, being more than three times as great in January and in excess of twice as large in July.

Of considerable interest is the transition zone in the vicinity of 50,000 feet where the European winds change from a double maxima pattern below to a single maximum above, while the North American profiles change in precisely the opposite direction from a single maximum below 50,000 feet to double maxima above.

In January the westerlies at 80,000 feet over Europe reach a broad maximum at 60°N, while in North America the major maximum is north of 70°N and there is a secondary peak at about 37°N. In July the winds are easterly above 50,000 feet at all latitudes over both Europe and North America. In Europe the easterlies vary only slightly with latitude from 25°N to 75°N. There is a flat maximum in the vicinity of 55°N. In contrast, the summer high-level easterlies over North America have two maxima, one north of 75°N and the other south of 25°N. As in the case of the winds below 50,000 feet, the upper-level winds over North America have a much larger range than the European winds, the range at 80,000 feet being more than six times as great in winter and five times as large in summer.

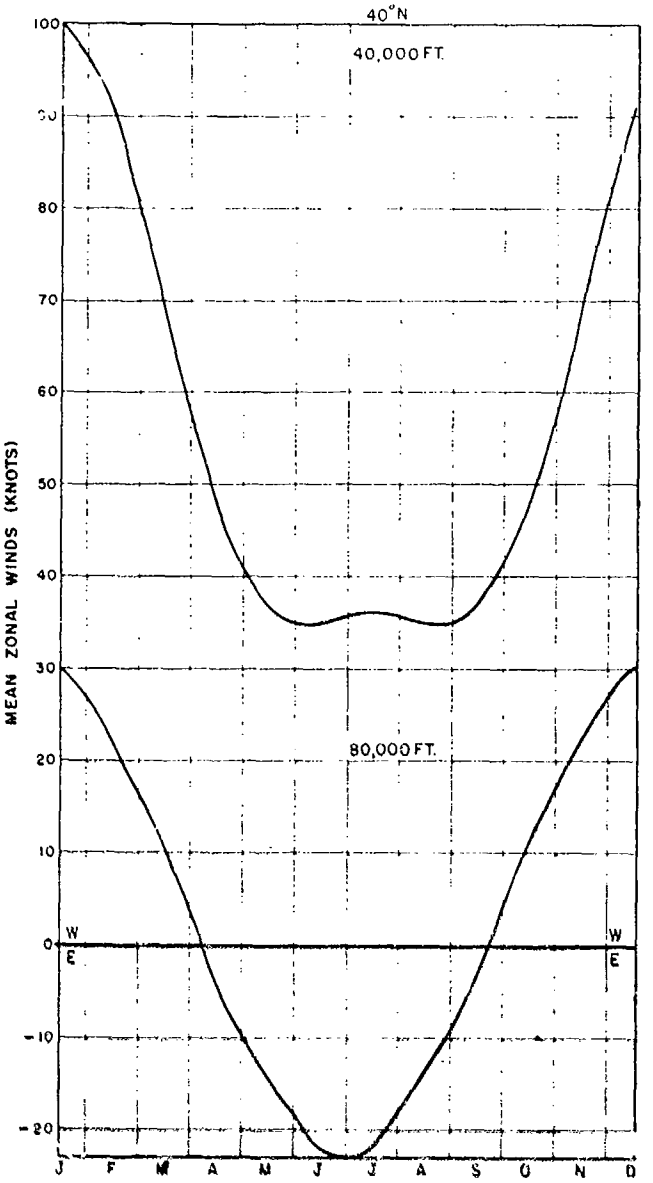

Figure 18. Seasonal variation of winds over North America

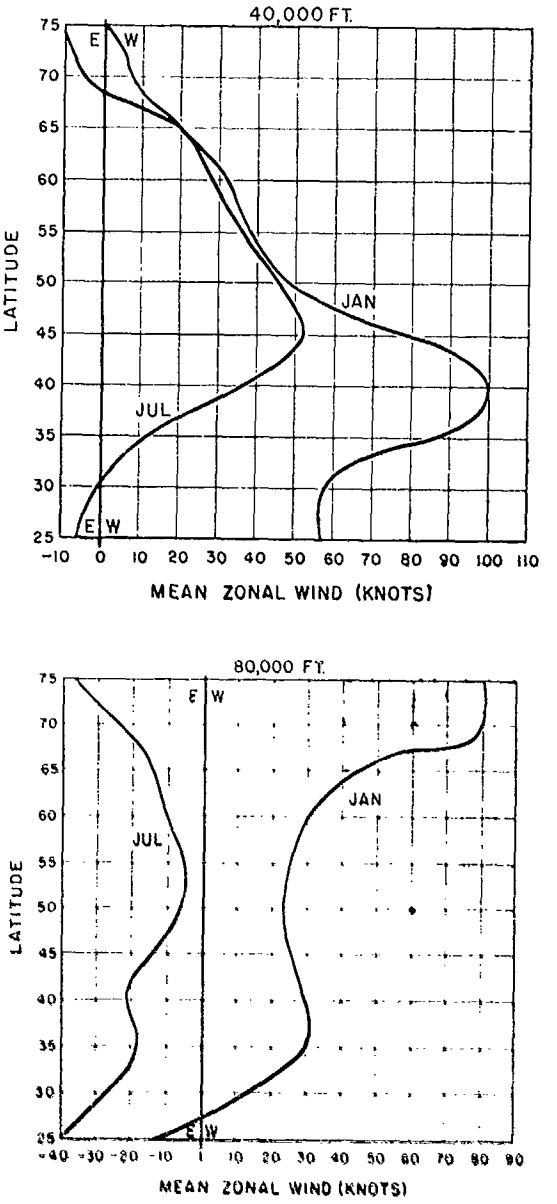

Figure 20. Latitudinal variation of winds over North America

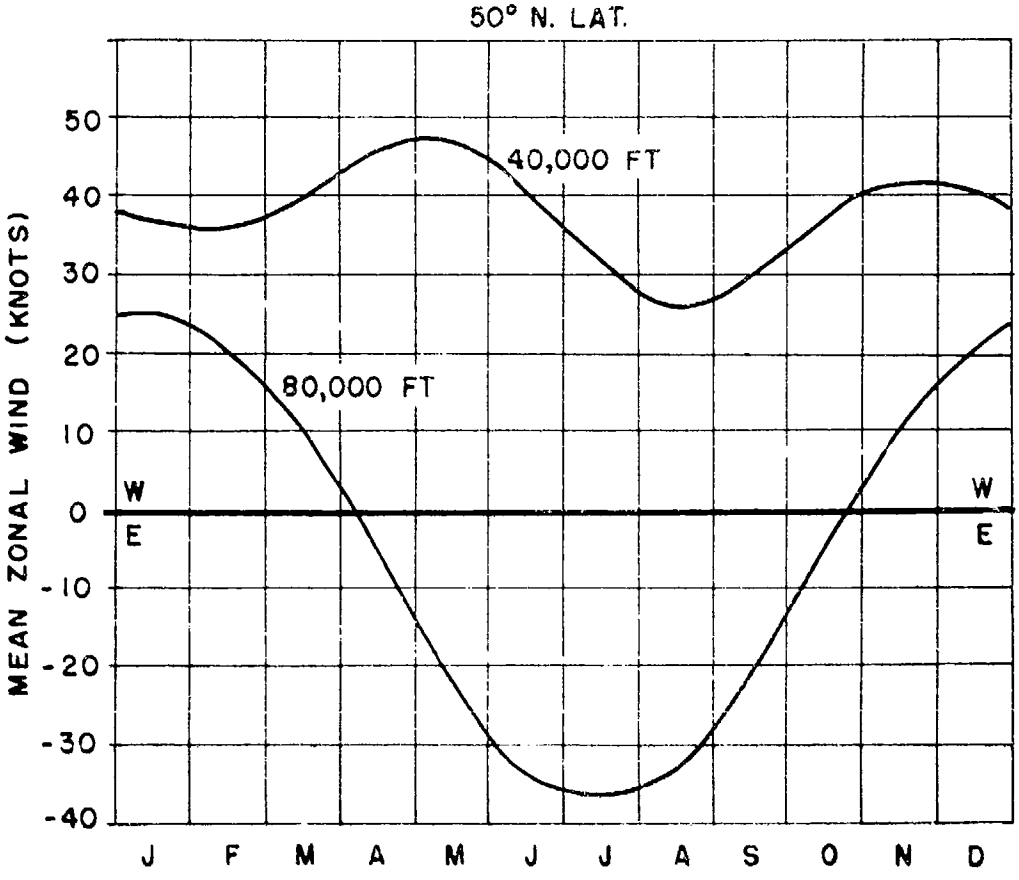

Figure 19. Seasonal variation of winds over Europe

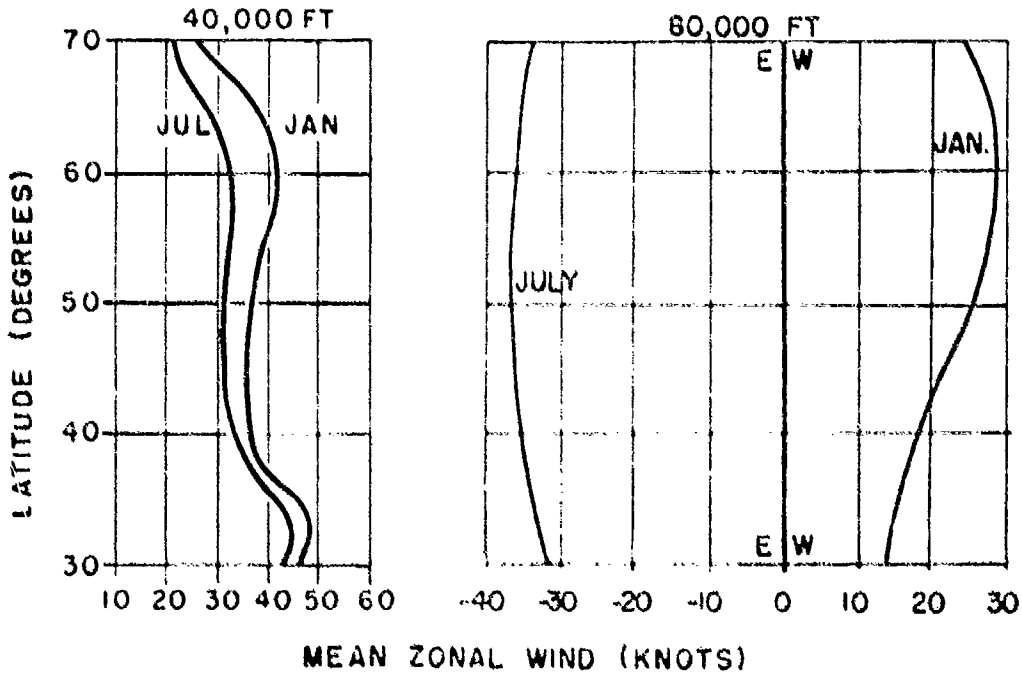

Figure 21. Latitudinal variation of winds over Europe

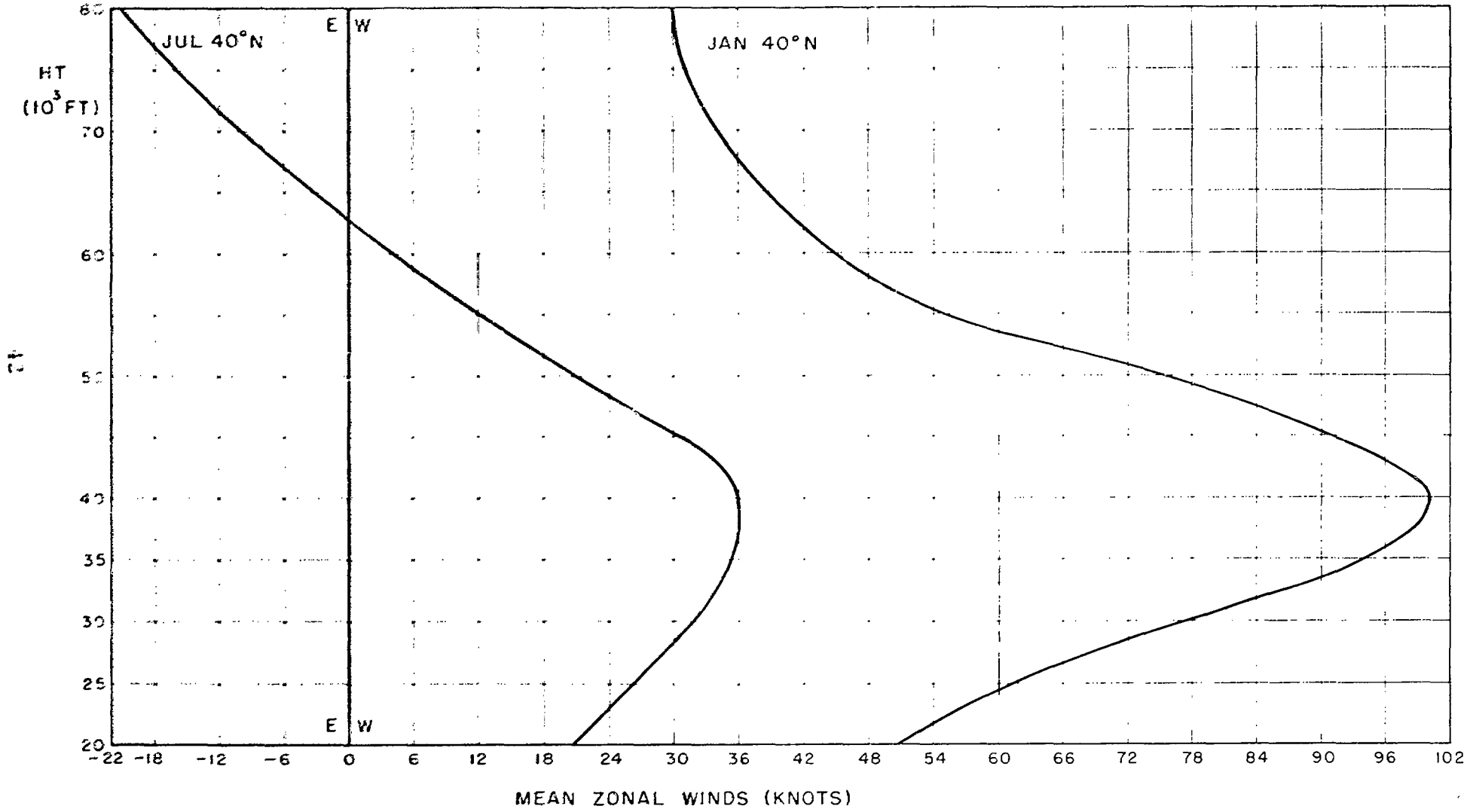

Figure 22. Vertical profile of winds over North America

3. VERTICAL VARIATION (Figures 22 and 23)

The variation with height of the mean zonal wind is similar for North America and Europe. The mean zonal wind reaches a maximum at 40,000 feet throughout the year between 25°N and 75°N. In January the wind decreases with height above 40,000 feet to a minimum, then increases again up to some level, presently unknown. Over Europe the minimum occurs at 70,000 feet; over North America, at 80,000 feet or above. The level of minimum wind does not appear to vary significantly with latitude. In July the wind also decreases with height above 40,000 feet. In the vicinity of 60,000 feet the direction reverses from West to East. Above this level the easterlies increase with height. Over North America, to the north of 70°N and to the south of 30°N, the winds are easterly at all levels in summer.

In middle latitudes in January the westerlies over North America are stronger at all levels than over Europe. The greatest difference occurs at 40,000 feet, the level of maximum wind, where a speed of 100 kts occurs in North America at 40°N as compared with 45 kts in Europe at 35°N. (Note the two latitudes selected for this comparison both lie along or near the horizontal axis of the mean wind maximum for the region in question.)

In summer it appears that the maximum easterlies occur above 80,000 feet in North America and near 80,000 feet in Europe. Of special interest is the fact that the high-level easterlies have the greatest constancy of all the wind regimes we have studied.

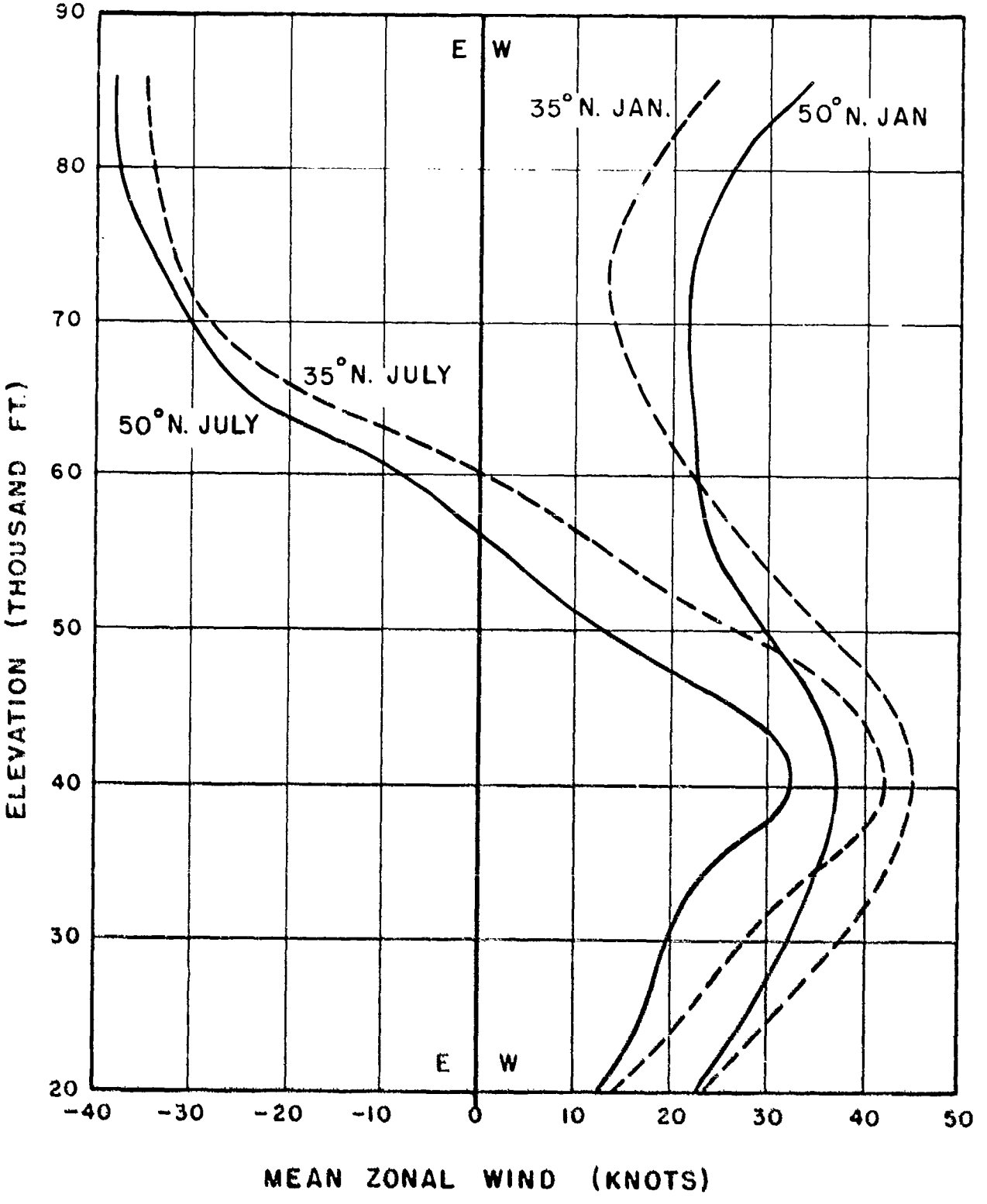

Figure 23. Vertical profile of winds over Europe

APPENDIX III

VARIATION OF THE STANDARD DEVIATION WITH TIME

We have adopted the classical diffusion theory developed by G. I. Tavlor.[1] He considered a fluid containing uniformly distributed, small-scale eddies which produce diffusion by continuous movement. We have adapted this theory to large-scale eddies of the general circulation.

If R_ξ is the correlation between u (the West - East wind component) at time t and u at time $t+\xi$, where ξ is a small time increment, then Taylor shows that

$$\sigma^2(x) = 2\sigma^2(u) \int_0^t \int_0^t R_\xi \, d\xi \, dt \qquad (1)$$

where $\sigma(x)$ is the standard deviation of x-displacements (that is, West - East displacements) and $\sigma(u)$ is the standard deviation of the wind.

The solution of this equation depends upon the form of the auto-correlation function, R_ξ. Brunt[9] derived the following exponential form for this function by considering a fluid where eddies are all the same size:

$$R_\xi = e^{-a\xi} \qquad (2)$$

where a is a constant depending on the size of the eddies.

Substituting Eq. (2) into Eq. (1):

$$\sigma^2(x) = 2\sigma^2(u) \int_0^T \int_0^t e^{-a\xi} \, d\xi \, dt .$$

Integrating

$$\frac{\sigma^2(x)}{\sigma^2(u)} = \frac{2T}{a} - \frac{2}{a^2}(1 - e^{-aT}) \qquad (3)$$

or

$$\frac{\sigma(x)}{\sigma(u)} = G(T) \qquad (4)$$

where

$$G(T) = \left[\frac{2T}{a} - \frac{2}{a^2}(1 - e^{-aT}) \right]^{1/2} \qquad (4a)$$

We have seen that the function G(T), which defines the ratio between $\sigma(x)$ and $\sigma(u)$, is obtained by integrating the auto-correlation function, R_ξ, twice with respect to time. If the eddies are all of one size then the auto-correlation function is exponential and the G-function has the form given in Eq. (4a).

Obviously, eddies in nature are not of a single size; therefore, R_ξ is not strictly exponential. However, the principal concern here is not the exact form of R_ξ, since any errors in this function are smoothed out by the double integration required to obtain G(T). The important consideration is the degree to which Eq. (4a) approximates the actual G-function.

To see if Eq. (4a) does in fact closely approximate the actual G-function, we computed G(T) directly in an Eulerian system of coordinates (where measurements are made at fixed points in space as time varies). The advantage of this system is that computations are made from actual wind data. This affords the opportunity of determining the G-function for as long a time period as desired.

Actually, we are interested in the G-function for a Lagrangean system (where measurements are taken along the path of a moving particle), but limited samples of trajectories restrict computation of the function to periods of only 2 or 3 days. However, there is no reason to assume that the form of the G-function will be different in the two systems. Therefore, we may use the Eulerian computations to determine the form of the G-function.

The Eulerian computations were made using German wind data at $50^{\circ}N$ for 225 millibars. Winds were resolved into u and v components and the ratios $\frac{\sigma(x)}{\sigma(u)}$ and $\frac{\sigma(y)}{\sigma(v)}$ were computed at 1-day intervals up to a period of 6 days. It was found that the two ratios have identical time variations, thus $G_x(T)=G_y(T)$. Furthermore, the G-function is very closely approximated by Eq. (4a) with $e^{-a} = 0.6$.

While there is every reason to expect that the form of the G-function is the same in both the Eulerian and Lagrangean systems, it should not be anticipated that the constant, e^{-a}, is the same in the two systems. In fact, we would expect this constant to be smaller in the Lagrangean system, since space as well as time variations are included in the computation of G(T). We will now discuss three separate estimates of the G-function in Lagrangean coordinates. All three estimates show the expected smaller value of the constant, e^{-a}.

A sample of 55 Moby Dick constant-level balloon trajectories at about 200 mb was used in conjunction with associated upper air charts to compute values of $\frac{\sigma(x)}{\sigma(u)} = G(T)$ for time intervals of 12, 24, and 36 hours. A value of $e^{-a} = 0.4$ was obtained.

Another value of e^{-a} was computed from trajectory distributions calculated by Spreen (unpublished report) from about 3000 geostrophic trajectories, constructed from upper-level charts of the West German Weather Service, Bad Kissingen, Germany.[8] The value $e^{-a} = 0.4$ was again obtained.

R. R. Rapp[10] computed an empirical distribution from a sample of 179 trajectories at 500 mb for two fall seasons. Using Taylor's development[1] and assuming that $e^{-a} = 0.5$, he calculated the circular normal distribution for the same sample. The χ^2 test revealed no significant difference between the empirical and theoretical distributions; therefore, Rapp concluded that the value $e^{-a} = 0.5$, which he had chosen, was reasonable.

On the basis of the above studies we chose $e^{-a} = 0.4$ as being the most representative value. Substituting this value into Eq. (3) we obtain:

$$\sigma(x, T) = \sqrt{2}\,\sigma(u)\left[\,1.0917T - 1.1919\,(1 - [0.4]^{T})\,\right]^{1/2} \qquad (5)$$

This equation specifies the variation of $\sigma(x)$ with time.

APPENDIX IV

SPHERICAL TRANSFORMATION

Consider a coordinate system $\bar{x}$, $\bar{y}$, and $\bar{z}$ on a spherical earth. This coordinate system is rotated relative to the conventional coordinates x, y, and z in such a way that the $\bar{x}$ and $\bar{z}$ axes are both inclined by an angle $\phi = \frac{\pi}{2} - \theta_o$ to the x and z axes, respectively, while the $\bar{y}$ axis coincides with the y axis. (See Figure 24.) The angle, θ_o, is a fixed latitude on the real earth.

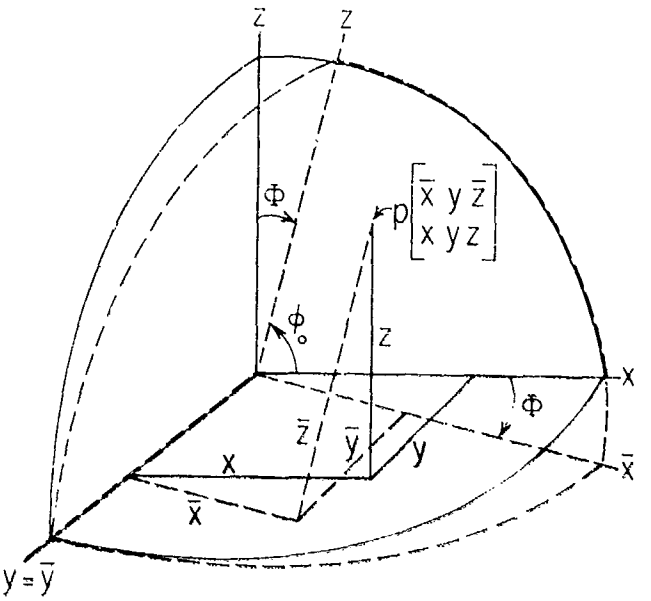

Figure 24. Spherical coordinates

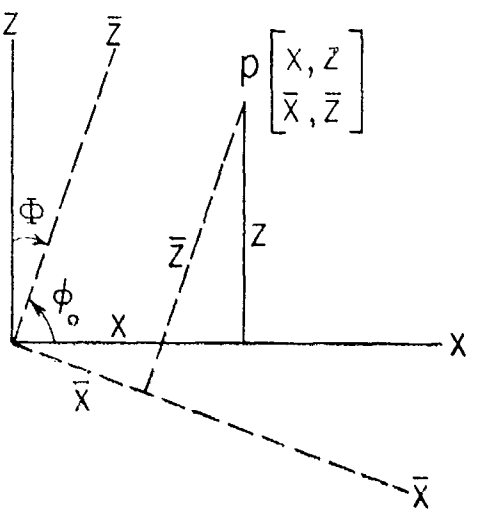

Figure 25. Axes x and z

Any arbitrary point, P, on the sphere has coordinates x, y, and z in the conventional system and x, y, and z in the rotated system. We wish to find the relationship between these two coordinate systems. Since $y = \bar{y}$, we already have one such relationship, hence the problem reduces to two dimensions. (See Figure 25.) Thus,

$$\begin{aligned} x &= \bar{x} \sin \theta_o + \bar{z} \cos \theta_o \\ y &= y \\ z &= \bar{z} \sin \theta_o - \bar{x} \cos \theta_o \quad . \end{aligned} \tag{1}$$

Introducing the following notation:

R, radius of the earth.

Angles (degrees):	Rotated System	Conventional System
	s, co-latitude	θ, latitude
	α, longitude	, longitude

In the rotated coordinate system:

$$\begin{aligned} x &= R \sin s \cos \alpha \\ \bar{y} &= R \sin s \sin \alpha \\ \bar{z} &= R \cos s \end{aligned} \tag{2}$$

In the conventional coordinate system:

$$\begin{aligned} x &= R \cos \phi \cos \lambda \\ y &= R \cos \phi \sin \lambda \\ z &= R \sin \phi \end{aligned} \tag{3}$$

Eliminate x, y, z and x, y, z from Eq. (1) by substituting Eqs. (2) and (3) to obtain ϕ and λ in terms of ϕ_o, s, and α.

The final result is:

$$\cos^2 \phi = \sin^2 s \left[1 - \cos^2 \phi_o (1 + \cos^2 \alpha) \right]$$

$$+ \cos^2 \phi_o + 1/2 \sin 2s \cos 2\phi_o \cos \alpha \tag{4}$$

$$\operatorname{ctn} \lambda = \operatorname{ctn} \alpha \sin \phi_o + \operatorname{ctn} s \cos \phi_o \csc \alpha \tag{5}$$

REFERENCES

1. Taylor, G. I., "Diffusion by Continuous Movement," Proc., Lond. Math. Soc. 20, Series 2, pp 196 (1922)

2. Solot, S. B. and Darling, E. M., Jr., 1958, Wind, Ch. 5, pp 5-56 to 5-73, Handbook of Geophysics for Air Force Designers, Geophysics Research Directorate, AFCRC (in preparation)

3. Brooks, C. E. P., Durst, C. S. Carruthers, N., et al, "Upper Winds Over the World," Met. Office, Geophysical Memoirs. No. 85, Vol 10, No. 5, M. O. 499C, London (1950)

4. Brooks, C. E. P., and Carruthers, N., Handbook of Statistical Methods in Meteorology, M. O. 538, Ch. 11, Her Majesty's Stationery Office, London (1953)

5. Buch, Hans S., "Hemispheric Wind Conditions During the Year 1950," Final Rpt Part 2, Gen. Circ. Proj. No. AF19(122)-153, Dept. of Meteorology, Massachusetts Institute of Technology, Cambridge (1954)

6. Court, Arnold, "Vertical Correlation of Wind Components," Sci. Rpt No. 1, AF19-604-2060, Cooperative Res. Found., Calif. (1951)

7. Solot, S. B. and Darling, E. M., Jr., "A Note on the Difference Method of Averaging," AMS Bulletin, Vol 35, pp 484-487 (1954)

8. Deutschen Wetterdienst in der US- Zone, 1950-1953: Taglicher Wetterbericht, Zentralami Bad Kissingen, Januar, April, Juli, Oktober

9. Brunt, David, Physical and Dynamical Meteorology, Ch. xii, Sect 157, pp 263-264, Camb. Univ. Press (1941)

10. Rapp, R. R., "The Distribution of the End Points of Air Trajectories," Rpt No. P-496-A, The Rand Corp., Santa Monica, Calif. (1954)

GEOPHYSICAL RESEARCH PAPERS

No. 1. Isotropic and Non-Isotropic Turbulence in the Atmospheric Surface Layer, Heinz Lettau, Geophysics Research Directorate, December 1949.

No. 2. Effective Radiation Temperatures of the Ozonosphere over New Mexico, Adel, Geophysics R-D, December 1949.

No. 3. Diffraction Effects in the Propagation of Compressional Waves in the Atmosphere, Norman A. Haskell, Geophysics Research Directorate, March 1950.

No. 4. Evaluation of Results of Joint Air Force-Weather Bureau Cloud Seeding Trials Conducted During Winter and Spring 1949, Charles E. Anderson, Geophysics Research Directorate, May 1950.

No. 5. Investigation of Stratosphere Winds and Temperatures From Acoustical Propagation Studies, Albert P. Crary, Geophysics Research Directorate, June 1950.

No. 6. Air-Coupled Flexural Waves in Floating Ice, F. Press, M. Ewing, A. P. Crary, S. Katz, and J. Oliver, Geophysics Research Directorate, November 1950.

No. 7. Proceedings of the Conference on Ionospheric Research (June 1949), edited by Bradford B. Underhill and Ralph J. Donaldson, Jr., Geophysics Research Directorate, December 1950.

No. 8. Proceedings of the Colloquium on Mesospheric Physics, edited by N. C. Gerson, Geophysics Research Directorate, July 1951.

No. 9. The Dispersion of Surface Waves on Multi-Layered Media, Norman A. Haskell, Geophysics Research Directorate, August 1951.

No. 10. The Measurement of Stratospheric Density Distribution with the Searchlight Technique, L. Elterman, Geophysics Research Directorate, December 1951.

No. 11. Proceedings of the Conference on Ionospheric Physics (July 1950) Part A, edited by N. C. Gerson and Ralph J. Donaldson, Jr., Geophysics Research Directorate, April 1952.

No. 12. Proceedings of the Conference on Ionospheric Physics (July 1950) Part B, edited by Ludwig Katz and N. C. Gerson, Geophysics Research Directorate, April 1952.

No. 13. Proceedings of the Colloquium on Microwave Meteorology, Aerosols and Cloud Physics, edited by Ralph J. Donaldson, Jr., Geophysics Research Directorate, May 1952.

No. 14. Atmospheric Flow Patterns and Their Representation by Spherical-Surface Harmonics, B. Haurwitz and Richard A. Craig, Geophysics Research Directorate, July 1952.

No. 15. Back-Scattering of Electromagnetic Waves From Spheres and Spherical Shells, A. L. Aden, Geophysics Research Directorate, July 1952.

No. 16. Notes on the Theory of Large-Scale Disturbances in Atmospheric Flow With Applications to Numerical Weather Prediction, Philip Duncan Thompson, Major, U. S. Air Force, Geophysics Research Directorate, July 1952.

No. 17. The Observed Mean Field of Motion of the Atmosphere, Yale Mintz and Gordon Dean, Geophysics Research Directorate, August 1952.

No. 18. The Distribution of Radiational Temperature Change in the Northern Hemisphere During March, Julius London, Geophysics Research Directorate, December 1952.

No. 19. International Symposium on Atmospheric Turbulence in the Boundary Layer, Massachusetts Institute of Technology, 4-8 June 1951, edited by E. W. Hewson, Geophysics Research Directorate, December 1952.

No. 20. On the Phenomenon of the Colored Sun, Especially the "Blue" Sun of September 1950, Rudolf Penndorf, Geophysics Research Directorate, April 1953.

No. 21. Absorption Coefficients of Several Atmospheric Gases, K. Watanabe, Murray Zelikoff and Edward C. Y. Inn, Geophysics Research Directorate, June 1953.

No. 22. Asymptotic Approximation for the Elastic Normal Modes in a Stratified Solid Medium, Norman A. Haskell, Geophysics Research Directorate, August 1953.

No. 23. Forecasting Relationships Between Upper Level Flow and Surface Meteorological Processes, J. J. George, R. O. Roche, H. B. Visscher, R. J. Shafer, P. W. Funke, W. R. Biggers and R. M. Whiting, Geophysics Research Directorate, August 1953.

No. 24. Contributions to the Study of Planetary Atmospheric Circulations, edited by Robert M. White, Geophysics Research Directorate, November 1953.

No. 25. The Vertical Distribution of Mie Particles in the Troposphere, R. Penndorf, Geophysics Research Directorate, March 1954.

No. 26. Study of Atmospheric Ions in a Nonequilibrium System, C. G. Stergis, Geophysics Research Directorate, April 1954.

No. 27. Investigation of Microbarometric Oscillations in Eastern Massachusetts, E. A. Flauraud, A. H. Mears, F. A. Crowley, Jr., and A. P. Crary, Geophysics Research Directorate, May 1954.

No. 28. The Rotation-Vibration Spectra of Ammonia in the 6- and 10-Micron Regions, R. G. Breene, Jr., Capt., USAF, Geophysics Research Directorate, June 1954.

No. 29. Seasonal Trends of Temperature, Density, and Pressure in the Stratosphere Obtained With the Searchlight Probing Technique, Louis Elterman, July 1954.

No. 30. Proceedings of the Conference on Auroral Physics, edited by N. C. Gerson, Geophysics Research Directorate, July 1954.

No. 31. Fog Modification by Cold-Water Seeding, Vernon G. Plank, Geophysics Research Directorate, August 1954.

GEOPHYSICAL RESEARCH PAPERS (Continued)

No. 32. Adsorption Studies of Heterogeneous Phase Transitions, S. J. Birstein, Geophysics Research Directorate, December 1954.

No. 33. The Latitudinal and Seasonal Variations of the Absorption of Solar Radiation by Ozone, J. Pressman, Geophysics Research Directorate, December 1954.

No. 34. Synoptic Analysis of Convection in a Rotating Cylinder, D. Fultz and J. Corn, Geophysics Research Directorate, January 1955.

No. 35. Balance Requirements of the General Circulation, V. P. Starr and R. M. White, Geophysics Research Directorate, December 1954.

No. 36. The Mean Molecular Weight of the Upper Atmosphere, Warren E. Thompson, Geophysics Research Directorate, May 1955.

No. 37. Proceedings on the Conference on Interfacial Phenomena and Nucleation.
I. Conference on Nucleation.
II. Conference on Nucleation and Surface Tension.
III. Conference on Adsorption.
Edited by H. Reiss, Geophysics Research Directorate, July 1955.

No. 38. The Stability of a Simple Baroclinic Flow With Horizontal Shear, Leon S. Pocinki, Geophysics Research Directorate, July 1955.

No. 39. The Chemistry and Vertical Distribution of the Oxides of Nitrogen in the Atmosphere, L. Miller, Geophysics Research Directorate, April 1955.

No. 40. Near Infrared Transmission Through Synthetic Atmospheres, J. N. Howard, Geophysics Research Directorate, November 1955.

No. 41. The Shift and Shape of Spectral Lines, R. G. Breene, Geophysics Research Directorate, October 1955.

No. 42. Proceedings on the Conference on Atmospheric Electricity, R. Holzer, W. Smith, Geophysics Research Directorate, December 1955.

No. 43. Methods and Results of Upper Atmospheric Research, J. Kaplan, G. Schilling, H. Kallman, Geophysics Research Directorate, November 1955.

No. 44. Luminous and Spectral Reflectance as Well as Colors of Natural Objects, R. Penndorf, Geophysics Research Directorate, February 1956.

No. 45. New Tables of Mie Scattering Functions for Spherical Particles, R. Penndorf, B. Goldberg, Geophysics Research Directorate, March 1956.

No. 46. Results of Numerical Forecasting With the Barotropic and Thermotropic Models, W. Gates, L. S. Pocinki, C. F. Jenkins, Geophysics Research Directorate, April 1956.

GEOPHYSICAL RESEARCH PAPERS (Continued)

No. 47. A Meteorological Analysis of Clear Air Turbulence (A Report on the U. S. Synoptic High-Altitude Gust Program), H. Lake, Geophysics Research Directorate, February 1956.

No. 48. A Review of Charge Transfer Processes in Gases, S. N. Ghosh, W. F. Sheridan, J. A. Dillon, Jr., and H. D. Edwards, Geophysics Research Directorate, July 1955.

No. 49. Theory of Motion of a Thin Metallic Cylinder Carrying a High Current, C. W. Dubs, Geophysics Research Directorate, October 1955.

No. 50. Hurricane Edna, 1954: Analysis of Radar, Aircraft, and Synoptic Data, E. Kessler, III and D. Atlas, Geophysics Research Directorate, July 1956.

No. 51. Cloud Refractive Index Studies, R. M. Cunningham, V. G. Plank, and C. F. Campen, Jr. Geophysics Research Directorate, October 1956.

No. 52. A Meteorological Study of Radar Angels, V. G. Plank, Geophysics Research Directorate, August 1956.

No. 53. The Construction and Use of Forecast Rejisters, I. Gringorten, I. Lund, M. Miller, Geophysics Research Directorate, June, 1956.

No. 54. Solar Geomagnetic Ionospheric Parameters as Indices of Solar Activity, F. Ward Jr., Geophysics Research Directorate, November, 1956.

No. 55. Preparation of Mutually Consistent Magnetic Charts, Paul Fougere, J. McClay, Geophysics Research Directorate, June 1957.

No. 56. Radar Synoptic Analysis of an Intense Winter Storm, Edwin Kessler III, Geophysics Research Directorate, October 1957.

No. 57. Mean Monthly 300 mb and 200 mb Contours and 500 mb, 300 mb, 200 mb Temperatures for the Northern Hemisphere, E. W. Wahl, April 1958.

No. 58. Theory of Large-Scale Atmospheric Diffusion and its Application to Air Trajectories, S. B. Solot and E. M. Darling, Jr., June 1958.

AD 152509

Air Force Cambridge Research Center
Geophysics Research Directorate
Bedford, Mass.

THEORY OF LARGE-SCALE ATMOSPHERIC DIFFUSION AND ITS APPLICATION TO AIR TRAJECTORIES." by S. B. Solot and E. M. Darling, Jr., June 1958. 51p. incl. illus. tables (Geophysical Research Papers No. 58; AFCRC-TR-58-228I)

Unclassified report

G. I. Taylor's theory of diffusion by continuous movement is adapted to motions on the scale of the general circulation. The resultant theory pertains to diffusion, by large-scale eddies, of air particles constrained to move on a constant-level surface. This theory provides a means for determining the probability field as a function of time for a particle originating from a given point on a sphere's surface. The bivariate normal density function describes

(over)

UNCLASSIFIED

1. Balloon Trajectory
2. Atmosphere - Motion
3. Atmosphere - Diffusion

I. Solot, S. B.
II. Darling, E. M., Jr.

AD 152509

Air Force Cambridge Research Center
Geophysics Research Directorate
Bedford, Mass.

THEORY OF LARGE-SCALE ATMOSPHERIC DIFFUSION AND ITS APPLICATION TO AIR TRAJECTORIES," by S. B. Solot and E. M. Darling, Jr., June 1958. 51p. incl. illus. tables (Geophysical Research Papers No. 58; AFCRC-TR-58-228I)

Unclassified report

G. I. Taylor's theory of diffusion by continuous movement is adapted to motions on the scale of the general circulation. The resultant theory pertains to diffusion, by large-scale eddies, of air particles constrained to move on a constant-level surface. This theory provides a means for determining the probability field as a function of time for a particle originating from a given point on a sphere's surface. The bivariate normal density function describes

(over)

UNCLASSIFIED

1. Balloon Trajectory
2. Atmosphere - Motion
3. Atmosphere - Diffusion

I. Solot, S. B.
II. Darling, E. M., Jr.

AD 152509

Air Force Cambridge Research Center
Geophysics Research Directorate
Bedford, Mass.

THEORY OF LARGE-SCALE ATMOSPHERIC DIFFUSION AND ITS APPLICATION TO AIR TRAJECTORIES," by S. B. Solot and E. M. Darling, Jr., June 1958. 51p. incl. illus. tables (Geophysical Research Papers No. 58; AFCRC-TR-58-228I)

Unclassified report

G. I. Taylor's theory of diffusion by continuous movement is adapted to motions on the scale of the general circulation. The resultant theory pertains to diffusion, by large-scale eddies, of air particles constrained to move on a constant-level surface. This theory provides a means for determining the probability field as a function of time for a particle originating from a given point on a sphere's surface. The bivariate normal density function describes

(over)

UNCLASSIFIED

1. Balloon Trajectory
2. Atmosphere - Motion
3. Atmosphere - Diffusion

I. Solot, S. B.
II. Darling, E. M., Jr.

UNCLASSIFIED

AD 152509
the probability of a displacement with West-East and North-South components. This function reduces to the circular normal form when suitable empirical and theoretical simplifications are introduced, concerning mean zonal wind, standard deviation of displacement components, and correlation between displacement component deviations. This density function is integrated in polar form and mapped on a projection of the earth's surface via a suitable spherical transformation. The resulting form of the distribution function is applicable to atomic fallout. In applying diffusion theory to balloon operations, the concept of downstream probability density function is introduced. This function defines probability density with respect to latitude of an East-West displacement at least as large as a specified value, occurring within T days. Downstream probability function tables are presented in Vol II (AD-152570) and Vol III (AD-152571) for (1) various constant values of mean wind and (2) North America and Eurasia for Jan, Apr, Jul and Oct at 40M to 80M ft.

UNCLASSIFIED

UNCLASSIFIED

AD 152509
the probability of a displacement with West-East and North-South components. This function reduces to the circular normal form when suitable empirical and theoretical simplifications are introduced, concerning mean zonal wind, standard deviation of displacement components, and correlation between displacement component deviations. This density function is integrated in polar form and mapped on a projection of the earth's surface via a suitable spherical transformation. The resulting form of the distribution function is applicable to atomic fallout. In applying diffusion theory to balloon operations, the concept of downstream probability density function is introduced. This function defines probability density with respect to latitude of an East-West displacement at least as large as a specified value, occurring within T days. Downstream probability function tables are presented in Vol II (AD-152570) and Vol III (AD-152571) for (1) various constant values of mean wind and (2) North America and Eurasia for Jan, Apr, Jul and Oct at 40M to 80M ft.

UNCLASSIFIED